

Long range two-particle rapidity correlations in A+A collisions from high energy QCD evolution

Kevin Dusling

*Physics Department, Building 510A
Brookhaven National Laboratory
Upton, NY-11973, USA
Email: kdusling@quark.phy.bnl.gov*

François Gelis

*Institut de Physique Théorique (URA 2306 du CNRS)
CEA/DSM/Saclay, Bât. 774
91191, Gif-sur-Yvette Cedex, France
Email: francois.gelis@cea.fr*

Tuomas Lappi

*Department of Physics, P.O. Box 35
40014 University of Jyväskylä, Finland
and
Helsinki Institute of Physics, P.O. Box 64,
00014 University of Helsinki, Finland
Email: tuomas.lappi@jyu.fi*

Raju Venugopalan

*Physics Department, Building 510A
Brookhaven National Laboratory
Upton, NY-11973, USA
Email: rajuv@mac.com*

ABSTRACT: Long range rapidity correlations in A+A collisions are sensitive to strong color field dynamics at early times after the collision. These can be computed in a factorization formalism [1] which expresses the n -gluon inclusive spectrum at arbitrary rapidity separations in terms of the multi-parton correlations in the nuclear wavefunctions. This formalism includes all radiative and rescattering contributions, to leading accuracy in $\alpha_s \Delta Y$, where ΔY is the rapidity separation between either one of the measured gluons and a projectile, or between the measured gluons themselves. In this paper, we use a mean field approximation for the evolution of the nuclear wavefunctions to obtain a compact result for inclusive two gluon correlations in terms of the unintegrated gluon distributions in the nuclear projectiles. The unintegrated gluon distributions satisfy the Balitsky-Kovchegov equation, which we solve with running coupling and with initial conditions constrained by existing data on electron-nucleus collisions. Our results are valid for arbitrary rapidity separations between measured gluons having transverse momenta $p_\perp, q_\perp \gtrsim Q_s$, where Q_s is the saturation scale in the nuclear wavefunctions. We compare our results to data on long range rapidity correlations observed in the near-side ridge at RHIC and make predictions for similar long range rapidity correlations at the LHC.

Contents

1. Introduction	1
2. Double inclusive gluon spectra at arbitrary rapidities	5
3. Gluon correlations from unintegrated gluon distributions	8
4. Running coupling BK evolution	12
5. Results for long range rapidity correlations in the Glasma	16
6. Summary	19
A. Evaluation of eq. (3.9)	20
B. Initial conditions for BK evolution	22

1. Introduction

In a high energy heavy ion collision, several thousand particles are produced in the initial interaction. The formation and evolution of the resulting fireball can be described in a framework where the incoming nuclei are sheets of strongly correlated coherent gluonic fields called Color Glass Condensates (CGC) [2–12], which are shattered in the collision to form strong classical fields called the Glasma [13–15]. The Glasma expands and thermalizes to form a nearly perfect quark-gluon fluid, which eventually hadronizes and freezes out to produce the large observed multiplicity of particles. While there is a fair amount of circumstantial evidence on the temporal evolution of latter stages of this space-time scenario, at present it is the earliest times, with the strongest “Glasma” fields, that are most amenable to a systematic theoretical treatment. This is because the early time dynamics at times of order $1/Q_s \lesssim 1$ fm is controlled by the saturation scale Q_s , which is the characteristic momentum scale in the evolution of the bulk matter produced in the collisions [16, 17]. Estimates for the magnitude of Q_s^2 are $1 - 1.4$ GeV² for gold nuclei at RHIC and $2.6 - 4$ GeV² for lead nuclei at LHC [18]. The existence of this semi-hard scale suggests that the Glasma may be described in weak coupling, thereby opening a new window into the study of strongly correlated quark-gluon matter.

The properties of the Glasma can be investigated by measuring long range rapidity correlations of particles produced in the collision. This is because the requirement that

correlations be causal requires the latest proper time τ_f that two particles could have been correlated to be¹

$$\tau_f = \tau_{f.o.} \exp\left(-\frac{1}{2}\Delta y\right), \quad (1.1)$$

where the freezeout time $\tau_{f.o.}$ is the proper time at which particles from the fireball have no further interactions and Δy is the rapidity separation between the two particles. Thus, for $\tau_{f.o.} \sim 10$ fm, two particles separated by 4 units in rapidity must have been correlated at no later than 1.4 fm. Strong correlations at space-time rapidity separations of $\Delta\eta \leq 4$ units have been observed in the “near-side ridge” correlations measured by the PHOBOS experiment at RHIC [19]. Correlations up to $\Delta\eta = 1.5$ have been extensively studied by the STAR collaboration [20]. At the LHC, multi-particle correlations at very large rapidity separations can be studied; these are correlations that must have been created at *proper times well below a fermi*, thereby providing a unique window into the non-linear dynamics of strong classical color fields in QCD.

It is therefore interesting to study the nature of these correlations and what they reveal about the Glasma. Further, since these correlations occur at very early times, after the collision, they are closely related to multi-parton correlations in the nuclear wavefunctions themselves. Multi-particle production in the Glasma, and its relation to correlations in the nuclear wavefunctions can be described in a weak coupling QCD framework where the degrees of freedom are strong color sources $\rho^a \sim 1/g$ in the nuclei (where g is the QCD coupling constant) and gauge fields. Before the collision, the distribution of sources and fields in the nuclear wavefunctions evolves with rapidity; the evolution equations for the color source distributions are the JIMWLK renormalization group equations [5–12]. After the collision, the color sources become time dependent, thereby enabling particle production in their radiation field. In Refs. [21,22], a field theory formalism was developed to compute moments of the multiplicity distribution in the Glasma systematically as an expansion in powers of g^2 , while simultaneously resumming contributions of order $g\rho \sim \mathcal{O}(1)$ from arbitrary numbers of insertions of color sources at each order in g^2 .

The naive expansion in powers of g^2 however breaks down because at each order there are large logarithmic contributions in $x_{1,2}$, the momentum fractions of partons in each of the nuclei, such that $g^2 \ln(1/x_{1,2}) \sim \mathcal{O}(1)$ at small $x_{1,2}$. These contributions therefore have to be resummed as well. In Refs. [1,23,24], it was shown that inclusive observables² in the Glasma can be expressed in a factorized form

$$\langle \mathcal{O} \rangle_{\text{LLog}} = \int [D\Omega_1(\bar{y}, \mathbf{x}_\perp) D\Omega_2(\bar{y}, \mathbf{x}_\perp)] W[\Omega_1(\bar{y}, \mathbf{x}_\perp)] W[\Omega_2(\bar{y}, \mathbf{x}_\perp)] \mathcal{O}_{\text{LO}}, \quad (1.2)$$

¹This expression is valid in the scenario when the space-time rapidity and momentum space rapidities are strongly correlated.

²This factorization is proven, to leading logarithmic accuracy in x , for inclusive multi-gluon spectra. It is straightforward to check that it applies to the expectation value of local operators such as the energy-momentum tensor $T^{\mu\nu}$, and multi-point correlations of such operators. It is unlikely to apply to exclusive final states that impose a veto on particle production in some regions of phase-space.

where the Wilson lines

$$\Omega_{1,2}(\bar{y}, \mathbf{x}_\perp) \equiv \text{P exp } ig \int_0^{x^\mp} dz^\mp \frac{1}{\nabla_\perp^2} \rho_{1,2}(z^\mp, \mathbf{x}_\perp). \quad (1.3)$$

are ordered in rapidity (or, equivalently, in the longitudinal coordinates x^\mp). In this definition of the Wilson line, the rapidity \bar{y} is measured from the fragmentation region of the projectiles³. The $\rho_{1,2}$ are the color source densities of the nuclei in Lorenz gauge at a given transverse co-ordinate \mathbf{x}_\perp and longitudinal position z^\mp . The W 's are universal weight functionals (diagonal elements of density matrices) that give the probability distribution of a given configuration of sources (or equivalently the Wilson lines $\Omega_{1,2}$).

If the separation scale between the sources and the fields in one of the nuclei (moving in the + direction) is Λ^+ , the requirement that the physics be independent of this cutoff gives rise to the JIMWLK renormalization group equation [5–12]

$$\frac{\partial}{\partial \ln(\Lambda^+)} W_{\Lambda^+}[\Omega_1] = -\mathcal{H}_{\Lambda^+} W_{\Lambda^+}[\Omega_1], \quad (1.4)$$

where H_{Λ^+} is the JIMWLK Hamiltonian at the cutoff scale Λ^+ . The precise form of the JIMWLK Hamiltonian is not needed in the rest of this paper, and we refer the reader to Refs. [5–12,23] for further details. The distributions $W[\Omega_{1,2}]$ that enter in eq. (1.2) are the limits when $\Lambda_\pm \rightarrow 0$ of the cutoff dependent distributions $W_{\Lambda_\pm}[\Omega_{1,2}]$

The “master” formula in eq. (1.2) is valid for all moments of the multiplicity distribution of gluons produced in the Glasma. Given a non-perturbative initial condition, the W weight functionals encode information about gluon correlations at all transverse positions and rapidities. A remarkable feature of eq. (1.2) is that the only “process dependent” input on the right hand side of the expression is the observable computed to leading order⁴ in α_s ; \mathcal{O}_{LO} , albeit non-perturbative, is obtained by solving classical Yang–Mills equations for the two nuclei and has been studied extensively for the single inclusive [25–33] gluon spectra using numerical lattice methods.

The Glasma Flux Tube picture of A+A collisions [34] is a consequence of this master formula. At short times after the collision, the solutions of the Yang–Mills equations

³It is therefore different from the usual laboratory frame rapidity y used as a measure of the longitudinal momentum of a particle in the final state of a reaction. For projectile 1, moving in the + z direction, they are related by $\bar{y} = Y_{\text{beam}} - y$, and for projectile 2 by $\bar{y} = -Y_{\text{beam}} - y$. The rapidity difference from the beam \bar{y} is related to the upper bound x^\mp in eq. (1.3) by $\bar{y} = \ln(P^\pm x^\mp)$ where P^\pm denotes the total longitudinal momentum of the projectiles 1 and 2 respectively.

⁴By leading order, we mean the first term in the expansion

$$\mathcal{O}[\rho_1, \rho_2] = \frac{1}{g^{2n}} [c_0 + c_1 g^2 + c_2 g^4 + \dots], \quad (1.5)$$

where each term corresponds to a different loop order. Each of the coefficients c_n is itself an infinite series of terms involving arbitrary orders in $(g\rho_{1,2})^p$. The “leading order” contribution,

$$\mathcal{O}_{\text{LO}}[\rho_1, \rho_2] \equiv \frac{c_0}{g^{2n}}, \quad (1.6)$$

corresponds to an infinite sum of tree diagrams.

provide longitudinal chromo-electric and chromo-magnetic fields in the forward light cone. In the McLerran–Venugopalan (MV) model [2–4], the distribution of color correlations in the nuclear weight functionals W is Gaussian with its width set by the saturation scale Q_s . The averaging over the weight functionals in eq. (1.2) ensures that only chromo-electric and magnetic fields localized in transverse areas of size $1/Q_s^2$ contribute to multi-particle production obtained by averaging over all events. In the MV model, color correlations extend to arbitrarily large rapidity intervals; this results in a picture of multi-particle production as arising from boost invariant flux tubes of size $1/Q_s^2$. This picture, albeit simple, gives a qualitative [34] and even semi-quantitative [35, 36] description of the near-side ridge correlations observed in the RHIC heavy ion experiments.

Reality however is more complex and the boost invariance of the Glasma flux tubes is violated both by quantum evolution effects (real gluon emissions and virtual corrections) in rapidity between the beam rapidity and the rapidities of the measured gluons and likewise by *quantum evolution between the measured gluons*. When the maximum rapidity interval between measured gluons $\Delta Y \ll 1/\alpha_s$, quantum radiation between the observed gluons is not significant and correlated gluon emission is approximately independent of ΔY . The factorization formalism for this case was developed in Refs. [23, 24]. A quantitative understanding of how correlations depend on ΔY , for arbitrary $\Delta Y \leq 2Y_{\text{beam}}$, requires that one understands the dynamics of real and virtual quantum corrections between the tagged gluons. As demonstrated in Ref. [1], all the necessary information is contained in eq. (1.2) and the general formula for two gluon correlations was derived in that paper.

In this paper, we will exploit the formalism of Ref. [1] to evaluate the rapidity dependence of correlated two gluon emission in A+A collisions at RHIC and LHC energies. Because solving the JIMWLK equation is highly computationally intensive [37], we will instead use a mean field approximation to this evolution equation known as the Balitsky–Kovchegov (BK) equation [38, 39]. The BK equation is a very good approximation to the JIMWLK equation [40], albeit it must be noted that this may be true only for a limited class of observables. Recently, significant progress has been made in computing Next-to-Leading-Order (NLO) contributions to the BK equation [41, 42] and the results have been successfully applied to phenomenological studies of HERA DIS data at small x [43, 44]. To apply this framework to nuclear collisions, we will first fix the initial conditions for the running coupling BK evolution of unintegrated gluon distributions for nuclei by fitting the existing inclusive e+A fixed target data. We will then apply our results to compute the rapidity dependence of two gluon correlations in A+A collisions.

Our paper is organized as follows. Readers interested primarily in the results of the paper can proceed directly to section 5. In section 2, we will restate the results of Ref. [1] for the single and double inclusive gluon spectrum and demonstrate how the expressions simplify vastly in the mean field BK approximation of quantum evolution. In section 3, the correlated two gluon distribution is expressed in terms of the unintegrated gluon distributions of nuclei. These distributions are determined in section 4 from numerical solutions of the BK equation with running coupling. To constrain the initial conditions for the evolution of these nuclear unintegrated distributions, we fit available fixed target e+A data — the initial conditions for proton unintegrated distributions were determined previously in

global fits to the HERA e+p data [43,44]. In section 5, we discuss our results for correlated two gluon production in the context of RHIC data from STAR and PHOBOS. We make predictions for what one may expect at the LHC. The final section contains our conclusions. Details of the computations, solutions of running coupling BK equations and fits to e+A fixed target data are contained in two appendices.

2. Double inclusive gluon spectra at arbitrary rapidities

The general leading log factorization formula (1.2) gives the distribution of gluons at *all* rapidities in the problem [1, 45, 46], including all the rapidity correlations in the leading log approximation. For single and double inclusive gluon production we only need the distribution of Wilson lines at one or two gluon rapidities respectively. We shall now specialize the generic formula (1.2) to the this specific case. The single inclusive gluon spectrum $dN_1/d^3\mathbf{p}$ at leading order depends only on the Wilson lines⁵ $\Omega_{1,2}(y, \mathbf{x}_\perp)$ at the rapidity $y = y_p$ of the produced gluon and not on the whole rapidity range contained in eq. (1.2). Therefore, we can simplify eq. (1.2) by inserting the identity

$$1 = \int [DU_{1,2}(\mathbf{x}_\perp)] \delta[U_{1,2}(\mathbf{x}_\perp) - \Omega_{1,2}(y_p, \mathbf{x}_\perp)] \quad (2.1)$$

and by defining the corresponding probability distributions for configurations of Wilson lines at the rapidity y_p

$$Z_{y_p}[U_{1,2}(\mathbf{x}_\perp)] \equiv \int [D\Omega_{1,2}(y, \mathbf{x}_\perp)] W[\Omega_{1,2}(y, \mathbf{x}_\perp)] \delta[U_{1,2}(\mathbf{x}_\perp) - \Omega_{1,2}(y_p, \mathbf{x}_\perp)] . \quad (2.2)$$

One then obtains the all order leading log result for the single inclusive gluon spectrum at the rapidity y_p to be

$$\left\langle \frac{dN_1}{d^2\mathbf{p}_\perp dy_p} \right\rangle_{\text{LLog}} = \int [DU_1(\mathbf{x}_\perp) DU_2(\mathbf{x}_\perp)] Z_{y_p}[U_1] Z_{y_p}[U_2] \left. \frac{dN_1[U_1, U_2]}{d^2\mathbf{p}_\perp dy_p} \right|_{\text{LO}} . \quad (2.3)$$

Note that the distribution $Z_{y_p}[U]$ obeys the JIMWLK equation,

$$\partial_{y_p} Z_{y_p}[U] = \mathcal{H}_{y_p} Z_{y_p}[U] , \quad (2.4)$$

which must be supplemented by an initial condition at a rapidity close to the fragmentation region of the projectiles. Eq. 2.3 is illustrated in figure 1.

As will become clear shortly, it is more convenient to express eq. (2.3) in terms of color charge densities as

$$\left\langle \frac{dN_1}{d^2\mathbf{p}_\perp dy_p} \right\rangle_{\text{LLog}} = \int [D\rho_1^p(\mathbf{x}_\perp) D\rho_2^p(\mathbf{x}_\perp)] Z_{y_p}[\rho_1^p] Z_{y_p}[\rho_2^p] \left. \frac{dN_1[\rho_1^p, \rho_2^p]}{d^2\mathbf{p}_\perp dy_p} \right|_{\text{LO}} . \quad (2.5)$$

⁵From here onwards, we shall use the standard definition of the rapidity y instead of the rapidity distance \bar{y} from the projectile. In terms of the Wilson lines introduced in the previous section, this translates to $\Omega_1(y, \mathbf{x}_\perp) = \Omega_1(Y_{\text{beam}} - \bar{y}, \mathbf{x}_\perp)$ and $\Omega_2(y, \mathbf{x}_\perp) = \Omega_2(\bar{y} + Y_{\text{beam}}, \mathbf{x}_\perp)$.

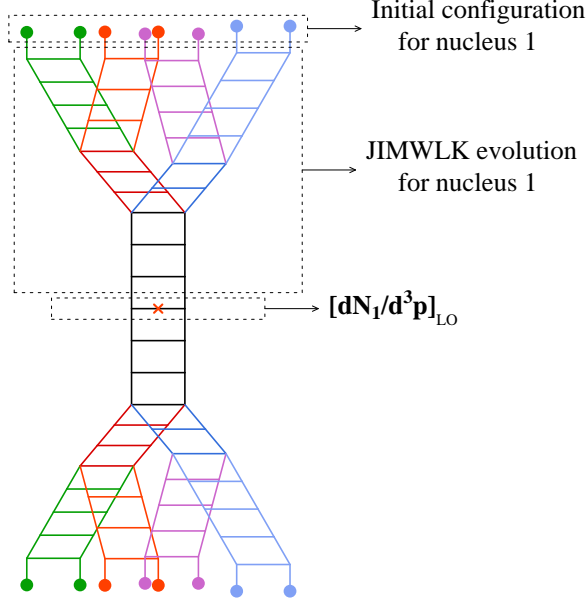


Figure 1: Diagrammatic representation of the various building blocks in the factorized formula for the inclusive single gluon spectrum. The lower part of the figure, representing nucleus 2, is made up of identical building blocks.

Here, the superscript on $\rho_{1,2}^p$ denotes the color charge distribution of nucleus 1 or 2 evaluated at the rapidity y_p .

Following a similar though slightly more involved derivation [1], one obtains from eq. (1.2) the expression

$$\begin{aligned}
\left\langle \frac{dN_2}{d^2\mathbf{p}_\perp dy_p d^2\mathbf{q}_\perp dy_q} \right\rangle_{\text{LLoG}} &= \int [D\rho_1^p(\mathbf{x}_\perp) D\rho_2^p(\mathbf{x}_\perp) D\rho_1^q(\mathbf{x}_\perp) D\rho_2^q(\mathbf{x}_\perp)] \\
&\quad \times Z_{y_p}[\rho_1^p] G_{y_p, y_q}[\rho_1^p, \rho_1^q] Z_{y_q}[\rho_2^q] G_{y_q, y_p}[\rho_2^q, \rho_2^p] \\
&\quad \times \left. \frac{dN_1[\rho_1^p, \rho_2^p]}{d^2\mathbf{p}_\perp dy_p} \right|_{\text{LO}} \left. \frac{dN_1[\rho_1^q, \rho_2^q]}{d^2\mathbf{q}_\perp dy_q} \right|_{\text{LO}} . \tag{2.6}
\end{aligned}$$

It is important to note that here we have taken $y_q > y_p$, where y_p is at an earlier stage in the evolution of projectile 1 and likewise, y_q is at an earlier stage in the evolution of projectile 2. This convention will be followed for the rest of this paper. Also, in eq. (2.6), $G_{y_q, y_p}[\rho_{1,2}^q, \rho_{1,2}^p]$ is a Green's function of the operator $\partial_y - \mathcal{H}_y$,

$$\partial_{y_q} G_{y_q, y_p}[U^q, U^p] = \mathcal{H}_{y_q} G_{y_q, y_p}[U^q, U^p] , \tag{2.7}$$

with the boundary condition

$$\lim_{y_q \rightarrow y_p} G_{y_q, y_p}[\rho^q, \rho^p] = \delta[\rho^q - \rho^p] . \tag{2.8}$$

This Green's function describes quantum evolution between two specified rapidities, in the presence of strong color fields from the projectiles. It relates the distribution of color

sources at a given rapidity with the distribution at another rapidity through the relation

$$\begin{aligned} Z_{y_q} [\rho_1^q] &= \int [D\rho_1^p] Z_{y_p} [\rho_1^p] G_{y_p, y_q} [\rho_1^p, \rho_1^q] \\ Z_{y_p} [\rho_2^p] &= \int [D\rho_2^q] Z_{y_q} [\rho_2^q] G_{y_q, y_p} [\rho_2^q, \rho_2^p] . \end{aligned} \quad (2.9)$$

At this stage, it is important to note that the BK mean field form of the Balitsky-JIMWLK evolution equation for the two point Wilson line correlator (the ‘‘dipole cross-section’’) requires that the correlator of the product of traces of two pairs of Wilson lines factorizes into the product of the correlators of traces of pairs of Wilson lines⁶,

$$\begin{aligned} &\left\langle \text{tr} [\tilde{U}^\dagger(\mathbf{x}_\perp) \tilde{U}(\mathbf{z}_\perp)] \text{tr} [\tilde{U}^\dagger(\mathbf{z}_\perp) \tilde{U}(\mathbf{y}_\perp)] \right\rangle \\ &= \left\langle \text{tr} [\tilde{U}^\dagger(\mathbf{x}_\perp) \tilde{U}(\mathbf{z}_\perp)] \right\rangle \left\langle \text{tr} [\tilde{U}^\dagger(\mathbf{z}_\perp) \tilde{U}(\mathbf{y}_\perp)] \right\rangle , \end{aligned} \quad (2.10)$$

to leading order in a $1/N_c$ expansion. The averages $\langle \dots \rangle$ are performed over the color sources of a large nucleus with the weight functional Z_y . The factorization in eq. (2.10) can be achieved with Gaussian correlations among the color sources. Note however that we need a non-local Gaussian distribution to accommodate the quantum BK evolution [47]. One obtains therefore⁷

$$Z_{y_p} [\rho_{1,2}^p] = \exp \left[-\frac{1}{2} \int_{\mathbf{x}_\perp, \mathbf{y}_\perp} \frac{\rho_{1,2}^{a,p}(\mathbf{x}_\perp) \rho_{1,2}^{a,p}(\mathbf{y}_\perp)}{\mu_{A_{1,2}}^2(y_p, \mathbf{x}_\perp - \mathbf{y}_\perp)} \right] , \quad (2.11)$$

where $\mu_{A_{1,2}}^2(y_p, \mathbf{x}_\perp - \mathbf{y}_\perp)$ represents the color charge squared per unit area of nucleus 1 or nucleus 2 as seen by a particle having rapidity y_p . Even though in this work we will consider collisions between identical nuclei, we shall retain the explicit $A_{1,2}$ notation for generality.

From eq. (2.9), because the Z_y functionals on the l.h.s and the r.h.s are both Gaussians, the Green’s function G_{y_q, y_p} must be Gaussian as well. One obtains

$$\begin{aligned} G_{y_p, y_q} [\rho_1^p, \rho_1^q] &= \exp \left[-\frac{1}{2} \int_{\mathbf{x}_\perp, \mathbf{y}_\perp} \frac{\Delta\rho_1(\mathbf{x}_\perp) \Delta\rho_1(\mathbf{y}_\perp)}{\Delta\mu_{A_1}^2(\mathbf{x}_\perp - \mathbf{y}_\perp)} \right] \\ G_{y_q, y_p} [\rho_2^q, \rho_2^p] &= \exp \left[-\frac{1}{2} \int_{\mathbf{x}_\perp, \mathbf{y}_\perp} \frac{\Delta\rho_2(\mathbf{x}_\perp) \Delta\rho_2(\mathbf{y}_\perp)}{\Delta\mu_{A_2}^2(\mathbf{x}_\perp - \mathbf{y}_\perp)} \right] , \end{aligned} \quad (2.12)$$

where we have defined

$$\begin{aligned} \Delta\rho_1(\mathbf{x}_\perp) &\equiv \rho_1^q(\mathbf{x}_\perp) - \rho_1^p(\mathbf{x}_\perp) \\ \Delta\rho_2(\mathbf{x}_\perp) &\equiv \rho_2^p(\mathbf{x}_\perp) - \rho_2^q(\mathbf{x}_\perp) \\ \Delta\mu_{A_1}^2(\mathbf{r}_\perp) &\equiv \mu_{A_1}^2(y_q, \mathbf{r}_\perp) - \mu_{A_1}^2(y_p, \mathbf{r}_\perp) \\ \Delta\mu_{A_2}^2(\mathbf{r}_\perp) &\equiv \mu_{A_2}^2(y_p, \mathbf{r}_\perp) - \mu_{A_2}^2(y_q, \mathbf{r}_\perp) . \end{aligned} \quad (2.13)$$

⁶These Wilson lines are defined in terms of the color charge densities through eq. (1.3) projected on to a particular rapidity $\tilde{U}(\mathbf{x}_\perp) \equiv \exp\left(ig\frac{1}{\sqrt{2}}\rho_a(\mathbf{x}_\perp)t^a\right)$, where the t^a ’s are the generators of the fundamental representation of $SU(N_c)$. The corresponding expression in the adjoint representation is given in eq. (3.6).

⁷It is to be understood that repeated color indices a are summed over.

Note that because of our choice $y_q > y_p$, $\Delta\mu^2$ as defined is always positive⁸.

Because the Green's functions in eq. (2.12) are expressed naturally as Gaussians in the new variables introduced in eq. (2.13), we can rewrite our general expression for the double inclusive distribution as

$$\begin{aligned} \left\langle \frac{dN_2}{d^2\mathbf{p}_\perp dy_p d^2\mathbf{q}_\perp dy_q} \right\rangle_{\text{LLog}} &= \int [D\rho_1^p(\mathbf{x}_\perp) D\rho_2^q(\mathbf{x}_\perp) D\Delta\rho_1(\mathbf{x}_\perp) D\Delta\rho_2(\mathbf{x}_\perp)] \\ &\times Z_{y_p}[\rho_1^p] G_{y_p, y_q}[\rho_1^p, \rho_1^q] Z_{y_q}[\rho_2^q] G_{y_q, y_p}[\rho_2^q, \rho_2^p] \\ &\times \left. \frac{dN_1[\rho_1^p, \rho_2^p]}{d^2\mathbf{p}_\perp dy_p} \right|_{\text{LO}} \left. \frac{dN_1[\rho_1^q, \rho_2^q]}{d^2\mathbf{q}_\perp dy_q} \right|_{\text{LO}}. \end{aligned} \quad (2.14)$$

With the Z_y 's from eq. (2.11) and the G_{y_q, y_p} 's from eq. (2.12), the only ingredient missing in obtaining a final expression for eq. (2.5) and eq. (2.14) is the expression of the leading order single inclusive spectrum in terms of the color charge densities of the two nuclei. This expression and the subsequent simplification of our equations for the inclusive distributions will be discussed in the next section.

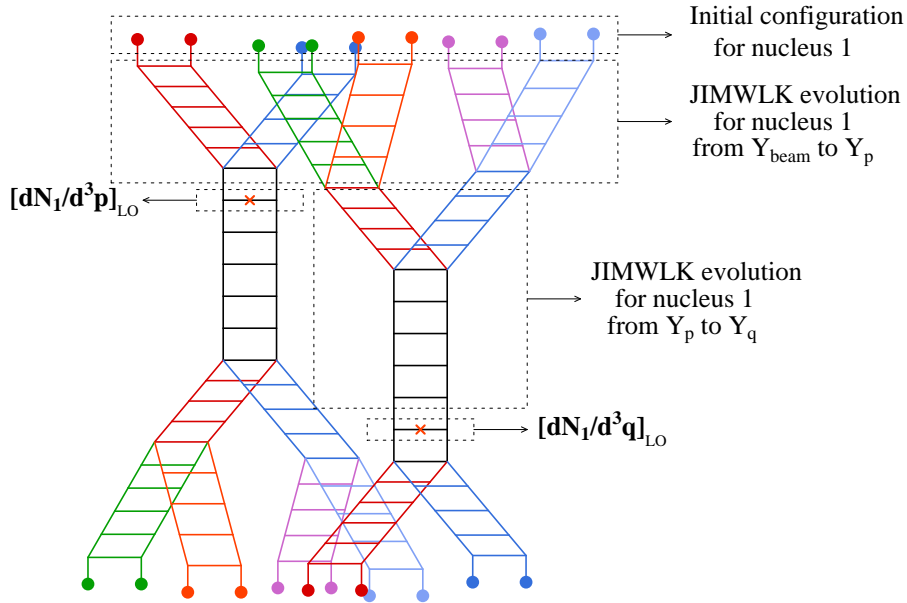


Figure 2: Diagrammatic representation of the various building blocks in the factorized formula for the inclusive 2-gluon spectrum. As in the previous figure, the corresponding evolution from nucleus 2 at the bottom of the figure is not shown explicitly.

3. Gluon correlations from unintegrated gluon distributions

The leading order single particle inclusive distribution, for a fixed distribution of sources,

⁸ μ_A^2 is proportional to the saturation scale, and therefore increases as one evolves away from the fragmentation region of a projectile.

is given by

$$\begin{aligned} \left. \frac{dN_1[\rho_1, \rho_2]}{d^2\mathbf{p}_\perp dy_p} \right|_{\text{LO}} &= \frac{1}{16\pi^3} \lim_{x_0, y_0 \rightarrow +\infty} \int d^3\mathbf{x} d^3\mathbf{y} e^{ip \cdot (x-y)} (\partial_x^0 - iE_p)(\partial_y^0 + iE_p) \\ &\quad \times \sum_{\lambda, a} \epsilon_\lambda^\mu(\mathbf{p}) \epsilon_\lambda^\nu(\mathbf{p}) A_\mu^a(x)[\rho_1, \rho_2] A_\nu^a(y)[\rho_1, \rho_2]. \end{aligned} \quad (3.1)$$

The gauge fields $A_\mu^a(x)[\rho_1, \rho_2]$ are solutions of the classical Yang-Mills equations in the forward light cone after the nuclear collision for a fixed configuration of sources $\rho_{1,2}^a$ in each of the nuclei. For Fourier modes \mathbf{k}_\perp of the color charge densities which obey $\tilde{\rho}_{1,2}(\mathbf{k}_\perp)/\mathbf{k}_\perp^2 \gtrsim 1$ (which is the case for $Q_s \gtrsim k_\perp$), only numerical solutions for $A_\mu(x)$ are known [25–33]. However, for $\tilde{\rho}_{1,2}/\mathbf{k}_\perp^2 \ll 1$, valid for $Q_s \ll k_\perp$, one can perturbatively expand the gauge field in powers of $\tilde{\rho}_{1,2}/\mathbf{k}_\perp^2$ and one obtains [48, 49]

$$p^2 A_a^\mu(\mathbf{p}) = -if_{abc} g^3 \int \frac{d^2\mathbf{k}_\perp}{(2\pi)^2} L^\mu(\mathbf{p}, \mathbf{k}_\perp) \frac{\tilde{\rho}_1^b(\mathbf{k}_\perp) \tilde{\rho}_2^c(\mathbf{p}_\perp - \mathbf{k}_\perp)}{\mathbf{k}_\perp^2 (\mathbf{p}_\perp - \mathbf{k}_\perp)^2} \quad (3.2)$$

where f_{abc} are the $SU(3)$ structure constants and $\tilde{\rho}_{1,2}$ are the Fourier transforms of the color charge densities of the two nuclei. Here L^μ is the well-known [50, 51] Lipatov vertex⁹.

For the single inclusive distribution in eq. (2.5), using eq. (3.1) and eq. (3.2) and the correlator

$$\langle \tilde{\rho}^a(\mathbf{k}_\perp) \tilde{\rho}^b(\mathbf{k}'_\perp) \rangle = (2\pi)^2 \mu_A^2(y) \delta^{ab} \delta(\mathbf{k}_\perp - \mathbf{k}'_\perp), \quad (3.3)$$

one obtains

$$\left\langle \frac{dN_1}{d^2\mathbf{p}_\perp dy_p} \right\rangle_{\text{LLog}} = S_\perp \frac{2g^6 N_c (N_c^2 - 1)}{(2\pi)^5} \frac{1}{\mathbf{p}_\perp^2} \int d^2\mathbf{k}_\perp \frac{\mu_{A_1}^2(y_p, \mathbf{k}_\perp) \mu_{A_2}^2(y_p, \mathbf{p}_\perp - \mathbf{k}_\perp)}{\mathbf{k}_\perp^2 (\mathbf{p}_\perp - \mathbf{k}_\perp)^2}, \quad (3.4)$$

where S_\perp is the transverse area of the overlap between the two nuclei. The unintegrated gluon distribution can be expressed as [47, 52, 53]

$$\phi_{A_{1,2}}(x, k_\perp) \equiv \frac{\pi R_{A_{1,2}}^2 \mathbf{k}_\perp^2}{4\alpha_s N_c} \int d^2\mathbf{x}_\perp e^{i\mathbf{k}_\perp \cdot \mathbf{x}_\perp} \langle \text{Tr} \left(U^\dagger(0) U(\mathbf{x}_\perp) \right) \rangle, \quad (3.5)$$

where the matrices U are adjoint Wilson lines evaluated in the classical color field created by a given partonic configuration of the nuclei A_1 or A_2 . For a nucleus moving in the $-z$ direction,

$$U(\mathbf{x}_\perp) \equiv \text{P}_+ \exp \left[ig \int_{-\infty}^{+\infty} dz^+ \frac{1}{\nabla_\perp^2} \rho_a(z^+, \mathbf{x}_\perp) T^a \right]. \quad (3.6)$$

Here the T^a are the generators of the adjoint representation of $SU(N_c)$ and P_+ denotes path ordering along the z^+ axis. At large \mathbf{k}_\perp , the Wilson lines can be expanded in powers of the sources to give, for Gaussian correlations,

$$\phi_A(y, \mathbf{k}_\perp) = g^2 \pi (\pi R_A^2) (N_c^2 - 1) \frac{\mu_A^2(y, \mathbf{k}_\perp)}{\mathbf{k}_\perp^2}. \quad (3.7)$$

⁹The components of the Lipatov four vector are $L^+(\mathbf{p}, \mathbf{k}_\perp) = -\frac{\mathbf{k}_\perp^2}{p^-}$, $L^-(\mathbf{p}, \mathbf{k}_\perp) = \frac{(\mathbf{p}_\perp - \mathbf{k}_\perp)^2 - \mathbf{p}_\perp^2}{p^+}$, $L^i(\mathbf{p}, \mathbf{k}_\perp) = -2\mathbf{k}_\perp^i$.

Substituting this relation in eq. (3.4), we obtain the well known \mathbf{k}_\perp -factorization expression [54, 55] for the single inclusive gluon distribution valid for $p_\perp \gg Q_s$:

$$\left\langle \frac{dN_1}{d^2\mathbf{p}_\perp dy_p} \right\rangle_{\text{LLog}} = \frac{2\alpha_s N_c S_\perp}{2\pi^4 (N_c^2 - 1) \mathbf{p}_\perp^2} \int \frac{d^2\mathbf{k}_\perp}{(2\pi)^2} \Phi_{A_1}(y_p, \mathbf{k}_\perp) \Phi_{A_2}(y_p, \mathbf{p}_\perp - \mathbf{k}_\perp), \quad (3.8)$$

where we denote $\Phi_A \equiv \phi_A / (\pi R_A^2)$ to be the unintegrated gluon distribution *per unit of transverse area*.

The corresponding expression for the double inclusive distribution is more involved. The r.h.s of eq. (2.14) has the product of two single inclusive distributions, one for a gluon with three momentum \mathbf{p} and likewise another for a gluon with three momentum \mathbf{q} . From eq. (3.1), this corresponds to the product of four gauge fields. As for the single inclusive case, the double inclusive gluon spectrum can be computed numerically using lattice techniques where Yang-Mills equations are solved to obtain the gauge fields as a function of proper time after the collision. This computation has been carried out recently for the Gaussian MV model [56]. Because this model does not include the effects of small x evolution, it is not ideal for the purpose of investigating the dynamics of long range rapidity correlations. Incorporating small x evolution effects in the non-perturbative computation is outside the scope of the present work. We will instead consider here, as in the previous discussion of the single inclusive distribution—see eq. (3.2), the perturbative limit of $p_\perp, q_\perp \gg Q_s$, where the gauge fields can be expanded as bilinear products of the color sources of the two nuclei. The dependence of the leading order double inclusive gluon spectrum on four gauge fields, then translates, in this perturbative limit to the product of eight color charge densities. The averages over color sources in eq. (2.14) are therefore averages over the general matrix element

$$\begin{aligned} \mathcal{F}^{bcdefghi}(\mathbf{p}, \mathbf{q}; \{\mathbf{k}_{i\perp}\}) &\equiv \left\langle \tilde{\rho}_1^{*f,p}(\mathbf{k}_{2\perp}) \tilde{\rho}_1^{*h,q}(\mathbf{k}_{4\perp}) \tilde{\rho}_1^{b,p}(\mathbf{k}_{1\perp}) \tilde{\rho}_1^{d,q}(\mathbf{k}_{3\perp}) \right. \\ &\quad \left. \times \tilde{\rho}_2^{*g,p}(\mathbf{p}_\perp - \mathbf{k}_{2\perp}) \tilde{\rho}_2^{*i,q}(\mathbf{q}_\perp - \mathbf{k}_{4\perp}) \tilde{\rho}_2^{c,p}(\mathbf{p}_\perp - \mathbf{k}_{1\perp}) \tilde{\rho}_2^{e,q}(\mathbf{q}_\perp - \mathbf{k}_{3\perp}) \right\rangle, \end{aligned} \quad (3.9)$$

where we denote by a superscript p or q the rapidity which the color sources correspond to. Further, these products of gauge fields contain bi-linear scalar products of the Lipatov vertices. These can be simplified [34, 57] and expressed as

$$\begin{aligned} \mathcal{G}(\mathbf{p}, \mathbf{q}; \{\mathbf{k}_{i\perp}\}) &= \frac{16}{(2\pi)^8} \frac{[(\mathbf{k}_{1\perp} \cdot \mathbf{p}_\perp - \mathbf{k}_{1\perp}^2)(\mathbf{k}_{2\perp} \cdot \mathbf{p}_\perp - \mathbf{k}_{2\perp}^2) + (\mathbf{k}_{1\perp} \times \mathbf{p}_\perp) \cdot (\mathbf{k}_{2\perp} \times \mathbf{p}_\perp)]}{\mathbf{k}_{1\perp}^2 \mathbf{k}_{2\perp}^2 \mathbf{p}_\perp^2 (\mathbf{p}_\perp - \mathbf{k}_{1\perp})^2 (\mathbf{p}_\perp - \mathbf{k}_{2\perp})^2} \\ &\quad \times \frac{[(\mathbf{k}_{3\perp} \cdot \mathbf{q}_\perp - \mathbf{k}_{3\perp}^2)(\mathbf{k}_{4\perp} \cdot \mathbf{q}_\perp - \mathbf{k}_{4\perp}^2) + (\mathbf{k}_{3\perp} \times \mathbf{q}_\perp) \cdot (\mathbf{k}_{4\perp} \times \mathbf{q}_\perp)]}{\mathbf{k}_{3\perp}^2 \mathbf{k}_{4\perp}^2 \mathbf{q}_\perp^2 (\mathbf{q}_\perp - \mathbf{k}_{3\perp})^2 (\mathbf{q}_\perp - \mathbf{k}_{4\perp})^2}. \end{aligned} \quad (3.10)$$

The double inclusive distribution in eq. (2.14), for transverse momenta $p_\perp, q_\perp \gg Q_s$, can therefore be expressed as

$$\left\langle \frac{dN_2}{d^2\mathbf{p}_\perp dy_p d^2\mathbf{q}_\perp dy_q} \right\rangle_{\text{LLog}} = \frac{g^{12}}{16(2\pi)^6} f^{abc} f^{a'de} f^{afg} f^{a'hi} \times \int \prod_{i=1}^4 d^2\mathbf{k}_{i\perp} \mathcal{G}(\mathbf{p}, \mathbf{q}; \{\mathbf{k}_{i\perp}\}) \mathcal{F}^{bcdefghi}(\mathbf{p}, \mathbf{q}; \{\mathbf{k}_{i\perp}\}), \quad (3.11)$$

in terms of $\mathcal{F}^{bcdefghi}(\mathbf{p}, \mathbf{q}; \{\mathbf{k}_{i\perp}\})$ and $\mathcal{G}(\mathbf{p}, \mathbf{q}; \{\mathbf{k}_{i\perp}\})$ defined above.

We shall now sketch how one evaluates these quantities with further details of the computation given in appendix A. We begin with the evaluation of the color averages in $\mathcal{F}^{bcdefghi}(\mathbf{p}, \mathbf{q}; \{\mathbf{k}_{i\perp}\})$. Because the Z 's in eq. (2.11) and the G in eq. (2.12) are Gaussian weight functionals, the relevant color source correlators are the equal rapidity correlators

$$\begin{aligned} \left\langle \tilde{\rho}_1^{*a,p}(\mathbf{k}_\perp) \tilde{\rho}_1^{b,p}(\mathbf{k}'_\perp) \right\rangle &= (2\pi)^2 \delta^{ab} \delta^2(\mathbf{k}_\perp - \mathbf{k}'_\perp) \mu_{A_1}^2(y_p, \mathbf{k}_\perp), \\ \left\langle \tilde{\rho}_2^{*a,q}(\mathbf{k}_\perp) \tilde{\rho}_2^{b,q}(\mathbf{k}'_\perp) \right\rangle &= (2\pi)^2 \delta^{ab} \delta^2(\mathbf{k}_\perp - \mathbf{k}'_\perp) \mu_{A_2}^2(y_q, \mathbf{k}_\perp), \\ \left\langle \Delta \tilde{\rho}_{1,2}^{*a}(\mathbf{k}_\perp) \Delta \tilde{\rho}_{1,2}^b(\mathbf{k}'_\perp) \right\rangle &= (2\pi)^2 \delta^{ab} \delta^2(\mathbf{k}_\perp - \mathbf{k}'_\perp) \Delta \mu_{A_{1,2}}^2(\mathbf{k}_\perp), \end{aligned} \quad (3.12)$$

and the non-equal rapidity correlators¹⁰

$$\begin{aligned} \left\langle \tilde{\rho}_1^{*a,q}(\mathbf{k}_\perp) \tilde{\rho}_1^{b,p}(\mathbf{k}'_\perp) \right\rangle &= \left\langle (\Delta \tilde{\rho}_1^*(\mathbf{k}_\perp) + \tilde{\rho}_1^{*a,p}(\mathbf{k}_\perp)) \tilde{\rho}_1^{b,p}(\mathbf{k}'_\perp) \right\rangle \\ &= (2\pi)^2 \delta^{ab} \delta^2(\mathbf{k}_\perp - \mathbf{k}'_\perp) \mu_{A_1}^2(y_p, \mathbf{k}_\perp), \\ \left\langle \tilde{\rho}_2^{*a,q}(\mathbf{k}_\perp) \tilde{\rho}_2^{b,p}(\mathbf{k}'_\perp) \right\rangle &= \left\langle \tilde{\rho}_2^{*a,q}(\mathbf{k}_\perp) (\Delta \tilde{\rho}_2^*(\mathbf{k}'_\perp) + \tilde{\rho}_2^{b,q}(\mathbf{k}'_\perp)) \right\rangle \\ &= (2\pi)^2 \delta^{ab} \delta^2(\mathbf{k}_\perp - \mathbf{k}'_\perp) \mu_{A_2}^2(y_q, \mathbf{k}_\perp). \end{aligned} \quad (3.13)$$

The correlators for the dependent variables ρ_1^q and ρ_2^p (see eq. (2.13)) are

$$\begin{aligned} \left\langle \tilde{\rho}_1^{*a,q}(\mathbf{k}_\perp) \tilde{\rho}_1^{b,q}(\mathbf{k}'_\perp) \right\rangle &= (2\pi)^2 \delta^{ab} \delta^2(\mathbf{k}_\perp - \mathbf{k}'_\perp) \mu_{A_1}^2(y_q, \mathbf{k}_\perp), \\ \left\langle \tilde{\rho}_2^{*a,p}(\mathbf{k}_\perp) \tilde{\rho}_2^{b,p}(\mathbf{k}'_\perp) \right\rangle &= (2\pi)^2 \delta^{ab} \delta^2(\mathbf{k}_\perp - \mathbf{k}'_\perp) \mu_{A_2}^2(y_p, \mathbf{k}_\perp). \end{aligned} \quad (3.14)$$

With the relations listed, we can now evaluate eq. (3.9). Simple combinatorics gives us a total of 9 possible pairwise contractions in eq. (3.9). The details of these are listed in appendix A. One of the contributions (eq. (A.1)) gives the non-correlated contribution to the two gluon inclusive distribution. Subtracting this term therefore results in the correlated two gluon inclusive distribution

$$C(\mathbf{p}, \mathbf{q}) \equiv \left\langle \frac{dN_2}{dy_p d^2\mathbf{p}_\perp dy_q d^2\mathbf{q}_\perp} \right\rangle - \left\langle \frac{dN}{dy_p d^2\mathbf{p}_\perp} \right\rangle \left\langle \frac{dN}{dy_q d^2\mathbf{q}_\perp} \right\rangle. \quad (3.15)$$

When one evaluates the other 8 terms that contribute to $C(\mathbf{p}, \mathbf{q})$, one observes that only 4 of these give leading contributions. The δ -function contributions from these terms (eqs. (A.2),

¹⁰This follows from the vanishing of terms odd in ρ or $\Delta\rho$.

(A.3), (A.4), (A.5)) give $\mathbf{k}_{1\perp} = \mathbf{k}_{2\perp}$ and $\mathbf{k}_{3\perp} = \mathbf{k}_{4\perp}$. Substituting this into the expression for $\mathcal{G}(\mathbf{p}, \mathbf{q}; \{\mathbf{k}_{i\perp}\})$ in eq. (3.10), one finds that it simplifies considerably to read

$$\mathcal{G}(\mathbf{p}, \mathbf{q}; \{\mathbf{k}_{i\perp}\}) = \frac{16}{(2\pi)^8 \mathbf{k}_{1\perp}^2 \mathbf{k}_{3\perp}^2 \mathbf{p}_\perp^2 \mathbf{q}_\perp^2 (\mathbf{p}_\perp - \mathbf{k}_{1\perp})^2 (\mathbf{q}_\perp - \mathbf{k}_{3\perp})^2} \quad (3.16)$$

Combining the four leading contributions from $\mathcal{F}^{bcdefghi}(\mathbf{p}, \mathbf{q}; \{\mathbf{k}_{i\perp}\})$ and the corresponding expressions from $\mathcal{G}(\mathbf{p}, \mathbf{q}; \{\mathbf{k}_{i\perp}\})$ to $C(\mathbf{p}, \mathbf{q})$ (see eqs. (A.10), (A.11), (A.12) and (A.13) in appendix A), we obtain

$$C(\mathbf{p}, \mathbf{q}) = \frac{\alpha_s^2}{16\pi^{10}} \frac{N_c^2(N_c^2 - 1)S_\perp}{d_A^4 \mathbf{p}_\perp^2 \mathbf{q}_\perp^2} \int d^2\mathbf{k}_{1\perp} \times \left\{ \begin{aligned} &\Phi_{A_1}^2(y_p, \mathbf{k}_{1\perp}) \Phi_{A_2}(y_p, \mathbf{p}_\perp - \mathbf{k}_{1\perp}) [\Phi_{A_2}(y_q, \mathbf{q}_\perp + \mathbf{k}_{1\perp}) + \Phi_{A_2}(y_q, \mathbf{q}_\perp - \mathbf{k}_{1\perp})] \\ &+ \Phi_{A_2}^2(y_q, \mathbf{k}_{1\perp}) \Phi_{A_1}(y_p, \mathbf{p}_\perp - \mathbf{k}_{1\perp}) [\Phi_{A_1}(y_q, \mathbf{q}_\perp + \mathbf{k}_{1\perp}) + \Phi_{A_1}(y_q, \mathbf{q}_\perp - \mathbf{k}_{1\perp})] \end{aligned} \right\}, \quad (3.17)$$

where the Φ 's are unintegrated gluon distributions per unit of transverse area and $d_A = N_c^2 - 1$. We have used here the relation between μ^2 and the unintegrated gluon distribution Φ given in eq. (3.7). This expression is the central result of this paper¹¹. We have obtained an expression for the double inclusive gluon distribution, valid to all orders in perturbation theory to leading logarithmic accuracy in x and for momenta $p_\perp, q_\perp \gg Q_s$, entirely in terms of the unintegrated gluon distributions of the two nuclei evaluated at the rapidities y_p and y_q where $y_p < y_q$. The corresponding expression for $y_p > y_q$ is obtained by replacing $A_1 \leftrightarrow A_2$ and $y_{p,q} \rightarrow -y_{p,q}$. We should emphasize that the notation used in eq. (3.17) stipulates that the un-integrated gluon distributions are evaluated at rapidities $y_{p,q} \pm Y_{\text{beam}}$.

4. Running coupling BK evolution

In the previous section, we established that the correlated two gluon spectrum for arbitrary rapidities can be computed in terms of the unintegrated gluon distributions of the two nuclei evaluated at these rapidities. In this section, we shall discuss how one computes this unintegrated gluon distribution and its evolution with x . In the next section, we shall use the results for the unintegrated gluon distribution to evaluate eq. (3.17) for the correlated inclusive two gluon distribution.

In eq. (3.5), we defined the unintegrated gluon distribution in a nucleus in terms of the correlator of two adjoint Wilson lines averaged over the color charge distribution in a nucleus. Because these averages $\langle \dots \rangle$ and those of correlators of fundamental Wilson lines are Gaussian correlators in the large N_c limit, one can express these correlators respectively

¹¹We note that expressions for the double inclusive cross-section have been previously derived [58] within the framework of Local Reggeon Field Theory [59]. At present the connection between the two frameworks is completely unclear.

as [52, 60]

$$\begin{aligned}\mathrm{Tr} \left\langle U(0)U^\dagger(\mathbf{r}_\perp) \right\rangle_Y &= N_c^2 e^{-C_A \Gamma(r_\perp, Y)} \\ \mathrm{Tr} \left\langle \tilde{U}(0)\tilde{U}^\dagger(\mathbf{r}_\perp) \right\rangle_Y &= N_c e^{-C_F \Gamma(r_\perp, Y)},\end{aligned}\quad (4.1)$$

where $C_A = N_c$ is the Casimir in the adjoint representation and $C_F = (N_c^2 - 1)/2N_c$ is the Casimir in the fundamental representation. The function Γ is closely related [47] to the variance of the non-local Gaussian weight functional in eq. (2.11) and is therefore the same in both the fundamental and adjoint cases. One can therefore, in the large N_c limit, simply express the correlator of two adjoint Wilson lines as the square of the correlator of two fundamental Wilson correlators.

The correlator of two Wilson lines in the fundamental representation is simply related to the dipole amplitude for the scattering of a quark-antiquark dipole (of transverse separation \mathbf{r}_\perp) off a nucleus as¹²

$$T(\mathbf{r}_\perp, Y) = 1 - \frac{1}{N_c} \mathrm{Tr} \left\langle \tilde{U}^\dagger(0)\tilde{U}(\mathbf{r}_\perp) \right\rangle_Y, \quad (4.2)$$

where \tilde{U} is a Wilson line in the fundamental representation. (See our previous discussion of these in the context of eq. (2.10).) Using eq. (4.1), one can write the unintegrated gluon distribution in the adjoint representation (per unit of transverse area) in eq. (3.5) as

$$\Phi_{A_{1,2}}(x, k_\perp) = \frac{\pi N_c k_\perp^2}{2\alpha_s} \int_0^{+\infty} r_\perp dr_\perp J_0(k_\perp r_\perp) [1 - T_{A_{1,2}}(r_\perp, \ln(1/x))]^2. \quad (4.3)$$

We therefore need to determine the dipole amplitude T and its evolution with rapidity $Y (= \ln(x_0/x))$ as an input in eq. (4.3) to extract the unintegrated gluon distribution. The dipole amplitude is obtained from the Balitsky-Kovchegov (BK) equation [38, 39], which is a non-linear evolution equation describing both gluon emission and multiple scattering effects in the interaction of the quark-antiquark dipole with a nucleus in the large N_c limit. It can be expressed as

$$\begin{aligned}\frac{\partial T(\mathbf{r}, Y)}{\partial Y} &= \int d\mathbf{r}_1 \mathcal{K}_{\mathrm{LO}}(\mathbf{r}, \mathbf{r}_1, \mathbf{r}_2) \times \\ &[T(\mathbf{r}_1, Y) + T(\mathbf{r}_2, Y) - T(\mathbf{r}, Y) - T(\mathbf{r}_1, Y)T(\mathbf{r}_2, Y)],\end{aligned}\quad (4.4)$$

with the leading order BFKL kernel [61] given by

$$\mathcal{K}_{\mathrm{LO}}(\mathbf{r}, \mathbf{r}_1, \mathbf{r}_2) = \frac{\alpha_s N_c}{2\pi^2} \frac{\mathbf{r}^2}{\mathbf{r}_1^2 \mathbf{r}_2^2}, \quad (4.5)$$

where $\mathbf{r}_2 \equiv \mathbf{r} - \mathbf{r}_1$. As we discussed previously, the BK equation for the amplitude is equivalent to the corresponding JIMWLK equation [5–12] of the Color Glass Condensate, in a mean field (large N_c) approximation where higher order dipole correlators are neglected.

¹²We assume translation invariance in the transverse plane to set the quark transverse coordinate to zero.

In the context of the BK equation, the leading order kernel corresponds to resumming the leading $(\alpha_s \ln(x_0/x))^n$ terms arising at small x from all orders in perturbation theory. It is well known however that running coupling contributions qualitatively modify the small x evolution beyond leading logarithms in x and there has been considerable recent work to include these corrections to the BK equation [41, 42]. The running coupling equation describing the evolution of the dipole amplitude however takes exactly the same form as eq. (4.4) with a modified evolution kernel given by

$$\mathcal{K}_{\text{Bal.}}(\mathbf{r}, \mathbf{r}_1, \mathbf{r}_2) = \frac{\alpha_s(\mathbf{r})N_c}{\pi} \left[\frac{\mathbf{r}^2}{\mathbf{r}_1^2 \mathbf{r}_2^2} + \frac{1}{\mathbf{r}_1^2} \left(\frac{\alpha_s(\mathbf{r}_1^2)}{\alpha_s(\mathbf{r}_2^2)} - 1 \right) + \frac{1}{\mathbf{r}_2^2} \left(\frac{\alpha_s(\mathbf{r}_2^2)}{\alpha_s(\mathbf{r}_1^2)} - 1 \right) \right]. \quad (4.6)$$

The subscript in $\mathcal{K}_{\text{Bal.}}$ refers to the ‘‘Balitsky prescription’’ for the evolution kernel, which corresponds to a scheme where some particular ultra-violet finite terms are also included along with the running coupling contributions to make the remainder numerically less important. For a more detailed discussion, we refer the reader to [62]. In this work, the NLO contributions not encompassed by the kernel in eq. (4.6) will be ignored. As argued previously [43], these contributions are systematically smaller than the running coupling contribution included here, especially at large rapidities.

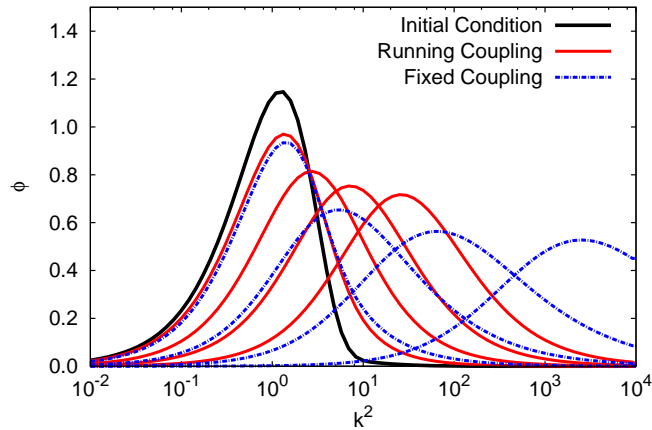


Figure 3: Unintegrated gluon distribution in the adjoint representation at $Y = 0, 2, 6, 10, 15$ (from left curve rightwards) with the Balitsky prescription for the kernel in eq. (4.6) as well as for the fixed coupling case. The distribution is in units of $N_c \pi R_A^2 / \alpha_s$.

In fig. 3, we show results for the unintegrated gluon distribution versus transverse momentum squared determined from the evolution with rapidity of the dipole amplitude in the adjoint representation (see eq. (4.3)) with i) the fixed coupling BK kernel, and ii) with the Balitsky prescription for the kernel in eq. (4.6)). As we will describe below, the initial conditions for the latter figure are constrained by fixed target e+A data. We note that the evolution of the unintegrated gluon distribution with Balitsky’s prescription for the running coupling effects is significantly slower than the evolution with a fixed coupling constant.

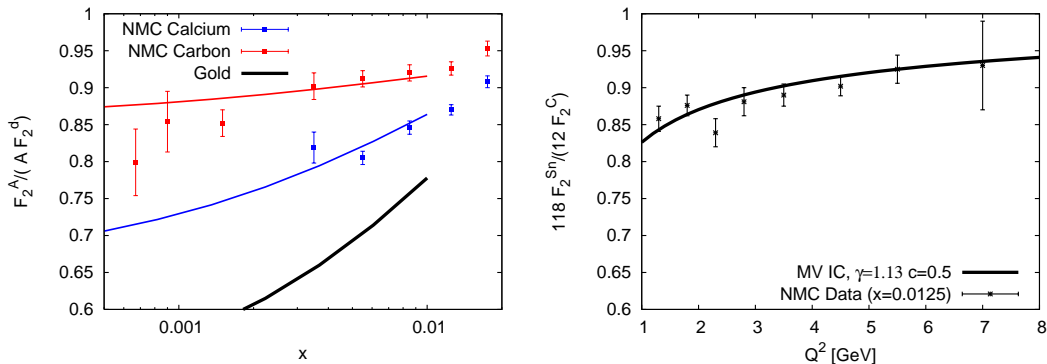


Figure 4: The x and Q^2 dependence of the normalized ratio of structure functions F_2 in nuclei. The curves in the left figure includes effects due to the small x evolution of the dipole cross-section described by the BK evolution with the modified kernel in eq. (4.6). The curve in the right figure is sensitive to the Q^2 dependence of the initial condition alone because it is evaluated at relatively large x . Details regarding the parameters of the initial condition are discussed in appendix B. The data are from the NMC collaboration [63].

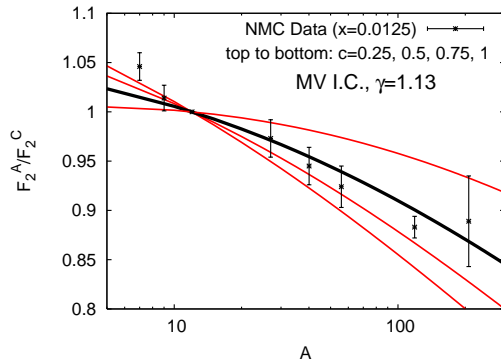


Figure 5: The A dependence of the ratio of structure functions given by data from the NMC collaboration [64]. The corresponding curves for other initial conditions are in appendix B.

The BK equation with the modified kernel in eq. (4.6) was first applied in Refs. [43,44] to a phenomenological study of the HERA data on the proton structure function F_2 . Two sets of initial conditions for the dipole amplitude at the initial rapidity $Y = Y_0$ were used—the GBW [65] and MV initial conditions [2–4]—and their parameters determined from fits to the HERA data. To constrain the initial conditions for nuclei and therefore extract the nuclear unintegrated gluon distribution, we performed a fit to the available NMC data on the nuclear structure function $F_{2,A}(x, Q^2)$. The details of the fit and the results are described in detail in appendix B. We show here in figs. 4 and 5 representative plots of fits to x , Q^2 and A dependence of the fixed target e+A data. Good fits to the available data are obtained for both sets of initial conditions for particular parameters. With the initial conditions for the BK equation fixed by the NMC data, we shall now use the corresponding unintegrated gluon distribution to study long range rapidity correlations in the Glasma.

5. Results for long range rapidity correlations in the Glasma

In this section, we will make use our result in eq. (3.17) for the double inclusive gluon distribution to compute long range rapidity correlations in A+A collisions at RHIC and the LHC. The essential ingredient in eq. (3.17) is the unintegrated gluon distribution which, as shown in eq. (4.3), is simply related to the dipole scattering amplitude. The evolution of the dipole scattering amplitude with rapidity (or x) is described by the BK evolution equation given in eq. (4.4), with the modified kernel given in eq. (4.6). The rapidity dependence of the double inclusive gluon spectrum therefore provides a sensitive test of high energy QCD evolution.

Equation (3.17) is derived in the leading $\ln x$ approximation, where all transverse momenta are assumed to be parametrically of the same order as Q_s . In this approximation the x -values at which the unintegrated gluon distributions are evaluated are not exactly determined, as long as $x \sim e^{\pm y} Q_s / \sqrt{s}$, where y is the appropriate rapidity of the produced gluon (y_p or y_q) and the sign depends on the nucleus (1 or 2) considered. We define the longitudinal momentum fractions of the produced gluons with respect to nucleus 1 or 2 (denoted by subscripts)

$$\begin{aligned} x_{1p} &= \frac{p_{\perp}}{\sqrt{s}} e^{-y_p} \quad ; \quad x_{1q} = \frac{q_{\perp}}{\sqrt{s}} e^{-y_q} \\ x_{2p} &= \frac{p_{\perp}}{\sqrt{s}} e^{+y_p} \quad ; \quad x_{2q} = \frac{q_{\perp}}{\sqrt{s}} e^{+y_q} \end{aligned} \quad (5.1)$$

In the above expression, p_{\perp} and q_{\perp} are the transverse momenta of the produced gluons. The unintegrated gluon distributions with momentum argument $\mathbf{p}_{\perp} \pm \mathbf{k}_{1\perp}$ and $\mathbf{q}_{\perp} \pm \mathbf{k}_{1\perp}$ in eq. (3.17) are evaluated at these values of the momentum fraction. For the unintegrated distribution with momentum argument $\mathbf{k}_{1\perp}$ we replace the transverse momentum in eq. (5.1) by $(\mathbf{p}_{\perp} + \mathbf{q}_{\perp})/2$ to make our evaluation of eq. (3.17) manifestly symmetric in \mathbf{p}_{\perp} and \mathbf{q}_{\perp} ¹³. Our derivation in Sec. 3 makes it clear that the term with Φ^2 in eq. (3.17) should be evaluated at a rapidity scale that is the *earlier* of the two rapidity scales y_p and y_q in the evolution of the corresponding nucleus. This prescription guarantees that the same is true when the scale is parametrized in terms of x instead of rapidity.

The solution of the BK equation is reliable when the gluon density is large. The initial condition for the evolution is typically set at $x \leq 0.01$. For larger values of x , one expects the BK description to break down; we use instead a phenomenological extrapolation (used previously in [47, 66]) for the unintegrated gluon distribution which has the form

$$\phi(x, \mathbf{k}_{\perp}) = \left(\frac{1-x}{1-x_0} \right)^{\beta} \phi(x_0, \mathbf{k}_{\perp}), \quad (5.2)$$

where $x_0 = 0.01$ and the parameter $\beta = 4$. This extrapolation to large x is unreliable and depends on physics which is not amenable to the renormalization group approach advocated here. However, in experiments with finite kinematic reach, it is inevitable that

¹³Another option would be to replace the momentum in eq. (5.1) by $Q_s(x)$. We have tried this and found our results to be insensitive to the choice of scale.

one is sensitive to the non-perturbative physics at large x in some kinematic range. For example, from the kinematic expressions in eq. (5.1), the unintegrated gluon distribution of gluons having $p_{\perp} = 0.5$ GeV at RHIC energies of $\sqrt{s} = 200$ GeV/nucleon will begin to be sensitive to the large x extrapolation of the distribution at $y_p \approx 1.4$ units in rapidity. At the LHC energy, the range in rapidity where we avoid this sensitivity is much greater. At $\sqrt{s} = 5.5$ TeV, the same gluon does not probe the large x extrapolation of the unintegrated gluon distribution until $y_p = 4.7$

With these caveats in mind, we shall now examine the two gluon inclusive distributions in A+A collisions both at RHIC ($\sqrt{s} = 200$ GeV) and at the LHC ($\sqrt{s} = 5.5$ TeV). The beam rapidities for these energies are $Y_{\text{beam}} \approx \pm \ln\left(\frac{\sqrt{s}}{M_{\text{nucleon}}}\right) \approx 5.36$ and 8.68 for RHIC and LHC respectively. We will first consider RHIC collisions and compare our results to recently measured long range rapidity correlations in the near-side ridge by the PHOBOS collaboration. The experimental quantity of interest is $\frac{1}{N_{\text{trig}}} \frac{dN}{d\Delta\eta}$, where the trigger particle consists of all particles having $p_{\perp} \geq 2.5$ GeV and an acceptance in rapidity in the range $0 \leq \eta^{\text{trig}} \leq 1.5$. The particles associated with this trigger have momenta larger than 4 (35) MeV at a rapidity of 3 (0). In performing the $\Delta\eta$ projection in the experiment, the near side yield is integrated over $|\Delta\phi_{pq}| \leq 1$. Hence in computing the per-trigger yield, we should in principle also integrate our two particle correlation $C(\mathbf{p}, \mathbf{q})$ over the PHOBOS acceptance. We will instead perform a more qualitative comparison here by computing instead our two particle correlation at representative values of the trigger and associated particle momenta and multiplying the result by the phase space volume corresponding to the PHOBOS acceptance.

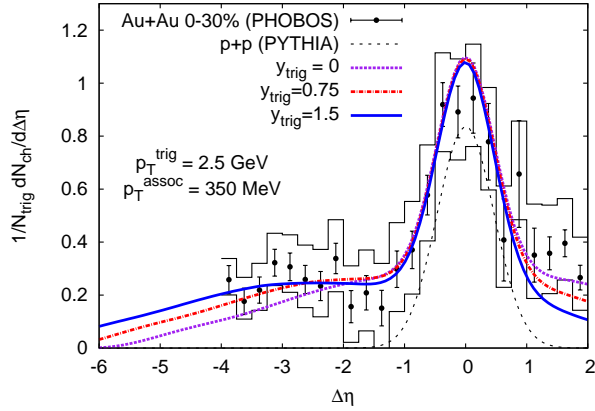


Figure 6: Comparison of our results for long range rapidity correlations to data from the PHOBOS collaboration [19]. The curves shown are obtained by adding our result (expressed by eq. (5.3) for long range rapidity correlations in the PHOBOS acceptance to the short range jet correlation in p+p collisions obtained using PYTHIA.

For the trigger particle we take $p_{\perp} = 2.5$ GeV at $y_{\text{trig}} = 0, 0.75$, and 1.5 units in rapidity. We assume the associated particle has mean $p_{\perp} = 350$ MeV. For all cases, we compute the yield at $\Delta\phi_{pq} = 0$. Then, in terms of our expression for the two particle

cumulant, the required quantity can be written as

$$\frac{1}{N_{\text{trig.}}} \frac{dN}{d\Delta\eta} \approx \mathcal{V}_{ps}^{\text{assoc.}} F(\Delta\phi_{pq} = 0) \frac{C(p_{\perp}^{\text{trig.}}, p_{\perp}^{\text{assoc.}}, y_{\text{trig.}}, y_{\text{assoc.}} = y_{\text{trig.}} + \Delta\eta, \Delta\phi_{pq} = 0)}{dN_1(p_{\perp}^{\text{trig.}}, y_{\text{trig.}})}, \quad (5.3)$$

where $C(\mathbf{p}, \mathbf{q})$ is the two particle cumulant given by eq. (3.17). In the above expression, the phase space volume corresponding to the trigger particle cancels out; we are left with an overall factor from the associated particle's phase space volume, $\mathcal{V}_{ps}^{\text{assoc.}}$, which we estimate to be $\mathcal{V}_{ps}^{\text{assoc.}} = \pi \text{ GeV}^2$. We arrive at this estimate by performing the angular integration over $\phi_{\text{assoc.}}$ times the p_{\perp} integration over the acceptance. Other than $\mathcal{V}_{ps}^{\text{assoc.}}$, the only additional parameter in our expression is $\alpha_s(Q_s^2)$ which we take to be $\alpha_s = 0.35$. With these stated values of α_s and $\mathcal{V}_{ps}^{\text{assoc.}}$, our overall normalization is now fixed. The function $F(\Delta\phi_{pq})$ comes from the collimation of the Glasma flux tubes due to radial flow as discussed in Ref. [34]. At $\Delta\phi_{pq} = 0$, this can be expressed as

$$F(\Delta\phi_{pq} = 0) = \cosh(\tanh^{-1} \beta) \quad (5.4)$$

where $\beta = V/c$ is the radial flow velocity.

To take into account the short range correlation from fragmentation not included in our formalism we add to eq. (5.3) the short range jet correlation resulting from PYTHIA. The result is compared to the PHOBOS experimental data [19] in fig. 6. One can see that the agreement with data is quite good. In principle the collimation from radial flow through eq. (5.4) can be a function of rapidity. We have estimated this effect by assuming that the space-time and momentum space rapidity are strongly correlated. From fits to BRAHMS data [67–69] on the inclusive hadron spectrum, we estimate the η dependence of the flow velocity to be $\beta(\eta) = 0.72 - 0.04|\eta|$. When including this rapidity dependent flow through eq. (5.4), the effect is so small that it would not result in a visible change to the curves plotted in figure 6.

At RHIC energies, the range in rapidity where the results are sensitive to small x physics exclusively is quite limited. At the LHC, this range is much larger and the effects of QCD evolution on long range rapidity correlations is more transparent. In fig. 7, we show results for the two particle cumulant $C(\mathbf{p}, \mathbf{q})$ as a function of the rapidity difference between the two gluons. In the figure on the left, the correlation is plotted for $p_{\perp} = q_{\perp} = 2 \text{ GeV}$; the right figure corresponds to the asymmetric case of $p_{\perp} = 10 \text{ GeV}$ and $q_{\perp} = 2 \text{ GeV}$. For both scenarios, we show the evolution in rapidity of the two particle correlation at different trigger rapidities y_p . The solid part of each curve corresponds to the kinematic range where only $x \leq 0.01$ values in each of the nuclear wavefunctions are being probed. In contrast, the dashed part of each curve denotes the kinematic range which is sensitive to $x > 0.01$ for at least one of the nuclei; in this regime, the results are more sensitive to the form chosen for the large x extrapolation than to the high energy QCD evolution equations at small x . Because of the large kinematic reach of the LHC, we observe in fig. 7 that we have a region contributing to the double inclusive rapidity spectrum, of nearly 7 units in the rapidity difference of the two gluons, which is sensitive only to the small x evolution in the nuclear wavefunctions. The shape and magnitude of these correlations will therefore give us unique insight into the evolution of multi-parton correlations in high energy QCD.

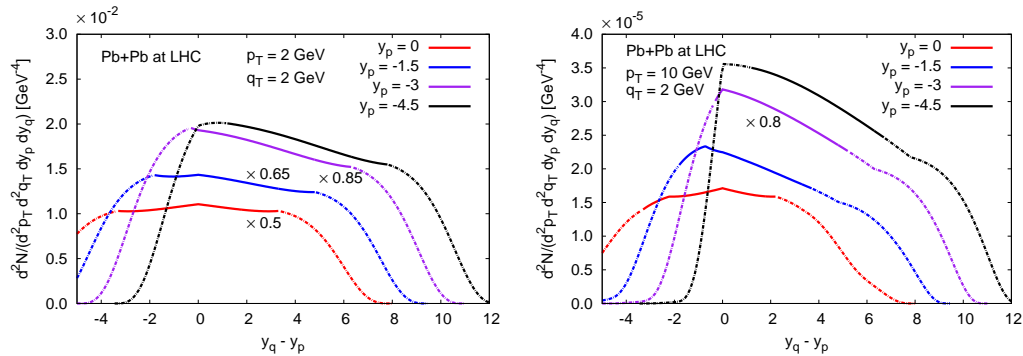


Figure 7: The predicted two particle correlation spectrum as a function of the rapidity difference between the two gluons. The figure on the left corresponds to the case where the transverse momenta of the two gluons are equal and are $p_{\perp}, q_{\perp} = 2$ GeV; the figure on the right depicts the case where $p_{\perp} = 10$ GeV and $q_{\perp} = 2$ GeV. The different plots reflect different trigger rapidities. Solid parts of each curve correspond to $x < 0.01$ in both nuclei; the dashed parts are sensitive to $x > 0.01$ in at least one of the nuclei. We have rescaled some curves, by the given factors, for clarity.

6. Summary

In Ref. [1], a general formula (eq. (2.6)) was derived for double inclusive gluon production in the Glasma at arbitrary rapidity separations. In this paper, we showed that this formula reduces to a compact expression, eq. (3.17), in terms of the unintegrated gluon distributions in the two nuclei. This simplification holds when $p_{\perp}, q_{\perp} \gtrsim Q_s$ and when the mean field Balitsky-Kovchegov (BK) framework — valid in the large N_c limit — is used to describe the high energy evolution of the nuclei. The unintegrated gluon distributions at small x are simply related to the dipole forward amplitude, which in turn satisfies the BK equation. Solving the running coupling form of the BK equation, with initial conditions determined from fits to fixed target e+A data, we computed the double inclusive spectrum at RHIC and LHC energies. In the case of the former, we obtained a good agreement with the PHOBOS data, albeit the kinematic region where small x partons are probed in both nuclei is rather small. In the latter case, we showed that there is a wide kinematic window for rapidity correlations at the LHC. Our results therefore open a new window into the study of the high energy evolution of multiparton correlations in nuclear wavefunctions.

Acknowledgements

We thank Javier Albacete, Adrian Dumitru, Anna Stasto and Kirill Tuchin for very useful discussions. We are especially grateful to Gregory Soyez for his co-ordinate space BK code. K.D. and R.V.'s research is supported by the US Department of Energy under DOE Contract No. DE-AC02-98CH10886. T.L. is supported by the Academy of Finland, project 126604. F.G. is supported in part by Agence Nationale de la Recherche via the program ANR-06-BLAN-0285-01.

A. Evaluation of eq. (3.9)

In this appendix, we work out some of the details of the derivation of the double inclusive spectrum. In particular, eq. (3.9) is expressed as the product of eight color charge densities. For a non-local Gaussian distribution of these sources, one has nine possible pairings of color source densities. These are evaluated explicitly below.

$$\begin{aligned} \mathcal{F}^{(9)} &= (2\pi)^8 \delta^{bf} \delta^{dh} \delta^{cg} \delta^{ei} \delta(\mathbf{k}_{1\perp} - \mathbf{k}_{2\perp}) \mu_{A_1}^2(y_p, |\mathbf{k}_{1\perp}|) \delta(\mathbf{k}_{3\perp} - \mathbf{k}_{4\perp}) \mu_{A_1}^2(y_q, |\mathbf{k}_{3\perp}|) \\ &\times \delta(\mathbf{k}_{2\perp} - \mathbf{k}_{1\perp}) \mu_{A_2}^2(y_p, |\mathbf{p}_\perp - \mathbf{k}_{1\perp}|) \\ &\times \delta(\mathbf{k}_{3\perp} - \mathbf{k}_{4\perp}) \mu_{A_2}^2(y_q, |\mathbf{q}_\perp - \mathbf{k}_{3\perp}|), \end{aligned} \quad (\text{A.1})$$

$$\begin{aligned} \mathcal{F}^{(1)} &= (2\pi)^8 \delta^{bf} \delta^{dh} \delta^{ce} \delta^{gi} \delta(\mathbf{k}_{1\perp} - \mathbf{k}_{2\perp}) \mu_{A_1}^2(y_p, |\mathbf{k}_{1\perp}|) \delta(\mathbf{k}_{3\perp} - \mathbf{k}_{4\perp}) \mu_{A_1}^2(y_q, |\mathbf{k}_{3\perp}|) \\ &\times \delta(\mathbf{q}_\perp + \mathbf{p}_\perp - \mathbf{k}_{3\perp} - \mathbf{k}_{1\perp}) \mu_{A_2}^2(y_q, |\mathbf{p}_\perp - \mathbf{k}_{1\perp}|) \\ &\times \delta(\mathbf{q}_\perp + \mathbf{p}_\perp - \mathbf{k}_{4\perp} - \mathbf{k}_{2\perp}) \mu_{A_2}^2(y_q, |\mathbf{p}_\perp - \mathbf{k}_{2\perp}|), \end{aligned} \quad (\text{A.2})$$

$$\begin{aligned} \mathcal{F}^{(2)} &= (2\pi)^8 \delta^{bf} \delta^{dh} \delta^{ci} \delta^{ge} \delta(\mathbf{k}_{1\perp} - \mathbf{k}_{2\perp}) \mu_{A_1}^2(y_p, |\mathbf{k}_{1\perp}|) \delta(\mathbf{k}_{3\perp} - \mathbf{k}_{4\perp}) \mu_{A_1}^2(y_q, |\mathbf{k}_{3\perp}|) \\ &\times \delta(\mathbf{p}_\perp - \mathbf{q}_\perp - \mathbf{k}_{2\perp} + \mathbf{k}_{3\perp}) \mu_{A_2}^2(y_q, |\mathbf{p}_\perp - \mathbf{k}_{2\perp}|) \\ &\times \delta(\mathbf{q}_\perp - \mathbf{p}_\perp - \mathbf{k}_{4\perp} + \mathbf{k}_{1\perp}) \mu_{A_2}^2(y_q, |\mathbf{p}_\perp - \mathbf{k}_{1\perp}|), \end{aligned} \quad (\text{A.3})$$

$$\begin{aligned} \mathcal{F}^{(3)} &= (2\pi)^8 \delta^{fh} \delta^{bd} \delta^{cg} \delta^{ie} \delta(\mathbf{k}_{2\perp} + \mathbf{k}_{4\perp}) \mu_{A_1}^2(y_p, |\mathbf{k}_{2\perp}|) \delta(\mathbf{k}_{1\perp} + \mathbf{k}_{3\perp}) \mu_{A_1}^2(y_p, |\mathbf{k}_{1\perp}|) \\ &\times \delta(\mathbf{k}_{1\perp} - \mathbf{k}_{2\perp}) \mu_{A_2}^2(y_p, |\mathbf{p}_\perp - \mathbf{k}_{1\perp}|) \\ &\times \delta(\mathbf{k}_{3\perp} - \mathbf{k}_{4\perp}) \mu_{A_2}^2(y_q, |\mathbf{q}_\perp - \mathbf{k}_{3\perp}|), \end{aligned} \quad (\text{A.4})$$

$$\begin{aligned} \mathcal{F}^{(6)} &= (2\pi)^8 \delta^{bh} \delta^{df} \delta^{cg} \delta^{ie} \delta(\mathbf{k}_{1\perp} - \mathbf{k}_{4\perp}) \mu_{A_1}^2(y_p, |\mathbf{k}_{1\perp}|) \delta(\mathbf{k}_{2\perp} - \mathbf{k}_{3\perp}) \mu_{A_1}^2(y_p, |\mathbf{k}_{2\perp}|) \\ &\times \delta(\mathbf{k}_{1\perp} - \mathbf{k}_{2\perp}) \mu_{A_2}^2(y_p, |\mathbf{p}_\perp - \mathbf{k}_{1\perp}|) \\ &\times \delta(\mathbf{k}_{3\perp} - \mathbf{k}_{4\perp}) \mu_{A_2}^2(y_q, |\mathbf{q}_\perp - \mathbf{k}_{3\perp}|), \end{aligned} \quad (\text{A.5})$$

$$\begin{aligned} \mathcal{F}^{(5)} &= (2\pi)^8 \delta^{fh} \delta^{bd} \delta^{ge} \delta^{ic} \delta(\mathbf{k}_{2\perp} + \mathbf{k}_{4\perp}) \mu_{A_1}^2(y_p, |\mathbf{k}_{2\perp}|) \delta(\mathbf{k}_{1\perp} + \mathbf{k}_{3\perp}) \mu_{A_1}^2(y_p, |\mathbf{k}_{1\perp}|) \\ &\times \delta(\mathbf{p}_\perp - \mathbf{q}_\perp - \mathbf{k}_{2\perp} + \mathbf{k}_{3\perp}) \mu_{A_2}^2(y_q, |\mathbf{p}_\perp - \mathbf{k}_{2\perp}|) \\ &\times \delta(\mathbf{q}_\perp - \mathbf{p}_\perp - \mathbf{k}_{4\perp} + \mathbf{k}_{1\perp}) \mu_{A_2}^2(y_q, |\mathbf{p}_\perp - \mathbf{k}_{1\perp}|), \end{aligned} \quad (\text{A.6})$$

$$\begin{aligned} \mathcal{F}^{(7)} &= (2\pi)^8 \delta^{fd} \delta^{bh} \delta^{ce} \delta^{gi} \delta(\mathbf{k}_{2\perp} - \mathbf{k}_{3\perp}) \mu_{A_1}^2(y_p, |\mathbf{k}_{2\perp}|) \delta(\mathbf{k}_{1\perp} - \mathbf{k}_{4\perp}) \mu_{A_1}^2(y_p, |\mathbf{k}_{1\perp}|) \\ &\times \delta(\mathbf{q}_\perp + \mathbf{p}_\perp - \mathbf{k}_{3\perp} - \mathbf{k}_{1\perp}) \mu_{A_2}^2(y_q, |\mathbf{p}_\perp - \mathbf{k}_{1\perp}|) \\ &\times \delta(\mathbf{q}_\perp + \mathbf{p}_\perp - \mathbf{k}_{4\perp} - \mathbf{k}_{2\perp}) \mu_{A_2}^2(y_q, |\mathbf{p}_\perp - \mathbf{k}_{2\perp}|), \end{aligned} \quad (\text{A.7})$$

$$\begin{aligned} \mathcal{F}^{(4)} &= (2\pi)^8 \delta^{fh} \delta^{bd} \delta^{ce} \delta^{gi} \delta(\mathbf{k}_{2\perp} + \mathbf{k}_{4\perp}) \mu_{A_1}^2(y_p, |\mathbf{k}_{2\perp}|) \delta(\mathbf{k}_{1\perp} + \mathbf{k}_{3\perp}) \mu_{A_1}^2(y_p, |\mathbf{k}_{1\perp}|) \\ &\times \delta(\mathbf{q}_\perp + \mathbf{p}_\perp - \mathbf{k}_{3\perp} - \mathbf{k}_{1\perp}) \mu_{A_2}^2(y_q, |\mathbf{p}_\perp - \mathbf{k}_{1\perp}|) \\ &\times \delta(\mathbf{q}_\perp + \mathbf{p}_\perp - \mathbf{k}_{4\perp} - \mathbf{k}_{2\perp}) \mu_{A_2}^2(y_q, |\mathbf{p}_\perp - \mathbf{k}_{2\perp}|), \end{aligned} \quad (\text{A.8})$$

and

$$\begin{aligned}
\mathcal{F}^{(8)} &= (2\pi)^8 \delta^{fd} \delta^{bh} \delta^{ge} \delta^{ic} \delta(\mathbf{k}_{2\perp} - \mathbf{k}_{3\perp}) \mu_{A_1}^2(y_p, |\mathbf{k}_{2\perp}|) \delta(\mathbf{k}_{1\perp} - \mathbf{k}_{4\perp}) \mu_{A_1}^2(y_p, |\mathbf{k}_{1\perp}|) \\
&\times \delta(\mathbf{p}_\perp - \mathbf{q}_\perp - \mathbf{k}_{2\perp} + \mathbf{k}_{3\perp}) \mu_{A_2}^2(y_q, |\mathbf{p}_\perp - \mathbf{k}_{2\perp}|) \\
&\times \delta(\mathbf{q}_\perp - \mathbf{p}_\perp - \mathbf{k}_{4\perp} + \mathbf{k}_{1\perp}) \mu_{A_2}^2(y_q, |\mathbf{p}_\perp - \mathbf{k}_{1\perp}|) .
\end{aligned} \tag{A.9}$$

The classification of these contributions was examined previously in [34] in the framework of the MV model. The analysis is identical here. The expression $\mathcal{F}^{(9)}$ is trivial as it cancels the square of the single particle distribution. Let us look at the δ -functions in $\mathcal{F}^{(4),(8)}$. These yield a local $[\delta(\mathbf{p}_\perp \pm \mathbf{q}_\perp)]^2$ -contribution that we shall neglect here as in Ref. [34]. Similarly, expressions $\mathcal{F}^{(5),(7)}$ are sub-dominant¹⁴. The leading terms are therefore $\mathcal{F}^{(1),(2),(3),(6)}$. If we plug these back into eq. (3.11), we obtain the following four contributions to the two gluon spectrum

$$\begin{aligned}
C^{(1)}(\mathbf{p}, \mathbf{q}) &= \frac{g^{12} N_c^2 (N_c^2 - 1) S_\perp}{16} \int d^2 \mathbf{k}_{1\perp} \mathcal{G}(\mathbf{p}, \mathbf{q}; \{\mathbf{k}_{i\perp}^{(1)}\}) \\
&\times \mu_{A_1}^2(y_p, |\mathbf{k}_{1\perp}|) \mu_{A_2}^4(y_q, |\mathbf{p}_\perp - \mathbf{k}_{1\perp}|) \mu_{A_1}^2(y_q, |\mathbf{p}_\perp + \mathbf{q}_\perp - \mathbf{k}_{1\perp}|) ,
\end{aligned} \tag{A.10}$$

where $\{\mathbf{k}_{i\perp}^{(1)}\} \equiv \{\mathbf{k}_{1\perp}, \mathbf{k}_{1\perp}, \mathbf{p}_\perp + \mathbf{q}_\perp - \mathbf{k}_{1\perp}, \mathbf{p}_\perp + \mathbf{q}_\perp - \mathbf{k}_{1\perp}\}$,

$$\begin{aligned}
C^{(3)}(\mathbf{p}, \mathbf{q}) &= \frac{g^{12} N_c^2 (N_c^2 - 1) S_\perp}{16} \int d^2 \mathbf{k}_{1\perp} \mathcal{G}(\mathbf{p}, \mathbf{q}; \{\mathbf{k}_{i\perp}^{(3)}\}) \\
&\times \mu_{A_1}^4(y_p, |\mathbf{k}_{1\perp}|) \mu_{A_2}^2(y_p, |\mathbf{p}_\perp - \mathbf{k}_{1\perp}|) \mu_{A_2}^2(y_q, |\mathbf{q}_\perp + \mathbf{k}_{1\perp}|) ,
\end{aligned} \tag{A.11}$$

where $\{\mathbf{k}_{i\perp}^{(3)}\} \equiv \{\mathbf{k}_{1\perp}, \mathbf{k}_{1\perp}, -\mathbf{k}_{1\perp}, -\mathbf{k}_{1\perp}\}$,

$$\begin{aligned}
C^{(2)}(\mathbf{p}, \mathbf{q}) &= \frac{g^{12} N_c^2 (N_c^2 - 1) S_\perp}{16} \int d^2 \mathbf{k}_{1\perp} \mathcal{G}(\mathbf{p}, \mathbf{q}; \{\mathbf{k}_{i\perp}^{(2)}\}) \\
&\times \mu_{A_1}^2(y_p, |\mathbf{k}_{1\perp}|) \mu_{A_2}^4(y_q, |\mathbf{p}_\perp - \mathbf{k}_{1\perp}|) \mu_{A_1}^2(y_q, |\mathbf{q}_\perp - \mathbf{p}_\perp + \mathbf{k}_{1\perp}|) ,
\end{aligned} \tag{A.12}$$

where $\{\mathbf{k}_{i\perp}^{(2)}\} \equiv \{\mathbf{k}_{1\perp}, \mathbf{k}_{1\perp}, \mathbf{q}_\perp - \mathbf{p}_\perp + \mathbf{k}_{1\perp}, \mathbf{q}_\perp - \mathbf{p}_\perp + \mathbf{k}_{1\perp}\}$, and finally

$$\begin{aligned}
C^{(6)}(\mathbf{p}, \mathbf{q}) &= \frac{g^{12} N_c^2 (N_c^2 - 1) S_\perp}{16} \int d^2 \mathbf{k}_{1\perp} \mathcal{G}(\mathbf{p}, \mathbf{q}; \{\mathbf{k}_{i\perp}^{(6)}\}) \\
&\times \mu_{A_1}^4(y_p, |\mathbf{k}_{1\perp}|) \mu_{A_2}^2(y_p, |\mathbf{p}_\perp - \mathbf{k}_{1\perp}|) \mu_{A_2}^2(y_q, |\mathbf{q}_\perp - \mathbf{k}_{1\perp}|) ,
\end{aligned} \tag{A.13}$$

where $\{\mathbf{k}_{i\perp}^{(6)}\} = \{\mathbf{k}_{1\perp}, \mathbf{k}_{1\perp}, \mathbf{k}_{1\perp}, \mathbf{k}_{1\perp}\}$. Using eq. (3.7), we can express $C^{(1)} + C^{(2)} + C^{(3)} + C^{(6)}$ as eq. (3.17).

¹⁴We note that there is an order one contribution coming from $\mathcal{F}^{(5),(7)}$ when the relative angle between p_\perp, q_\perp is $\Delta\phi_{pq} \lesssim \frac{Q_s}{p_\perp}$. In the limit where $\frac{Q_s}{p_\perp} \ll 1$ these contributions will be washed out by re-scattering in the same manner as the δ -function contributions coming from $\mathcal{F}^{(4),(8)}$, and thereby not alter our result. We thank Kirill Tuchin for pointing out this subtlety to us.

B. Initial conditions for BK evolution

The initial conditions for BK evolution of protons and nuclei are obtained by comparing results for the dipole cross-section to deep inelastic scattering data. The inclusive structure function F_2 is given by

$$F_2^A(x, Q^2) = \frac{Q^2}{4\pi^2\alpha_{em}} (\sigma_A^T + \sigma_A^L), \quad (\text{B.1})$$

where $\sigma_A^{T,L}$ is the virtual photon-nucleus cross section for transverse and longitudinal polarizations of the virtual photon. These in turn are given by

$$\sigma_A^{T,L}(x, Q^2) = \int_0^1 dz \int d^2\mathbf{b} d^2\mathbf{r} |\Psi_{T,L}(z, Q^2, \mathbf{r})|^2 \mathcal{N}_A(\mathbf{b}, \mathbf{r}, x), \quad (\text{B.2})$$

where \mathcal{N}_A is the dipole-nucleus scattering amplitude. We assume here that the \mathbf{b} dependence can be factorized as

$$\mathcal{N}_A(\mathbf{b}, \mathbf{r}, x) = 2\mathcal{T}_A(\mathbf{b}) \mathcal{N}_A(\mathbf{r}, x) \quad (\text{B.3})$$

The virtual photon-nucleus cross section can then be expressed as

$$\sigma_A^{T,L}(x, Q^2) = \sigma_A \int_0^1 dz \int d^2\mathbf{r} |\Psi_{T,L}(z, Q^2, \mathbf{r})|^2 \mathcal{N}_A(\mathbf{r}, x) \quad (\text{B.4})$$

where

$$\sigma_A = 2 \int d^2\mathbf{b} \mathcal{T}_A(\mathbf{b}) \quad (\text{B.5})$$

Initial condition for protons

The initial condition for protons was determined from a global fit of F_2 data in the work of [43]. Two different models for the initial condition were used in that work. The first is the GBW model

$$N(r, Y = 0) = 1 - \exp\left[-\frac{Q_{s_0}^2 r^2}{4}\right] \quad (\text{B.6})$$

and the other is the MV model

$$N(r, Y = 0) = 1 - \exp\left[-\left(\frac{Q_{s_0}^2 r^2}{4}\right)^\gamma \ln\left(\frac{1}{r^2 \Lambda_{QCD}^2} + e\right)\right] \quad (\text{B.7})$$

The fit parameters obtained in [43] are summarized in the table 1.

Initial condition for nuclei

We shall now consider the initial conditions for nuclei using the same model as the initial conditions for protons. We do not attempt to perform a global fit since the data for DIS

I.C.	σ_p (fm ²)	$Q_{s0,p}^2$ (GeV ²)	C^2	γ
GBW	3.159	0.24	5.3	NA
MV	3.277	0.15	6.5	1.13

Table 1: Parameters for the initial condition of the proton dipole cross section obtained in [43].

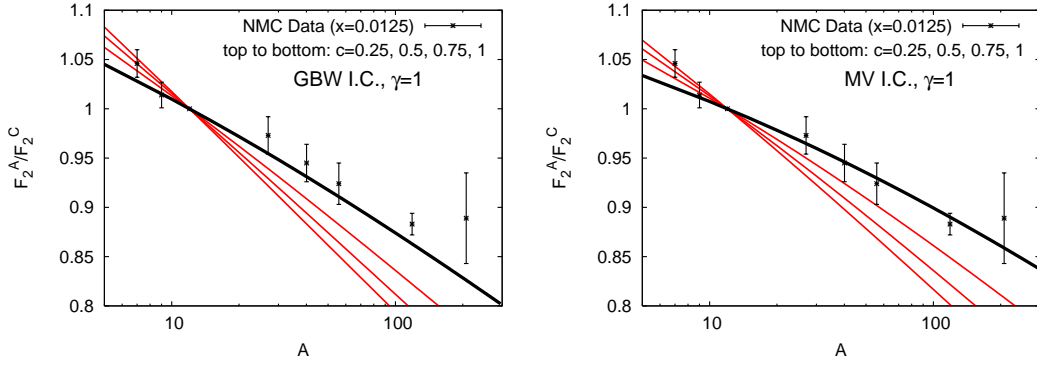


Figure 8: DIS fixed target e+A data on the ratio of structure functions as a function of A for fixed $x = 0.0125$. The plots correspond to (right) MV model initial condition having $\gamma = 1$ and (left) GBW initial condition.

off nuclei are not nearly of the same quality. We use a model where the initial saturation scale scales linearly with $A^{1/3}$,

$$Q_{s0}^2 = c A^{1/3} Q_{s0,p}^2, \quad (\text{B.8})$$

where c is a constant to be determined from the data.

In order to constrain the initial condition, we begin by looking at the New Muon Collaboration's (NMC) data [64] for F_2^A/F_2^C as a function of A at $x = 0.0125$ which is close to our $x_0 = 0.01$. In this case, there is no BK evolution, and we have a direct comparison of the nuclei's initial condition with the data. In computing F_2^A/F_2^C we will need a model for how the cross section scales with A . We take $\sigma_A = \left(\frac{A}{12}\right)^{2/3} \sigma_C$. Figure 8 shows the NMC data as a function of A for the GBW initial condition for four different values of c (left) and the MV model initial condition having anomalous dimension $\gamma = 1$ (right). It is clear that in order to be consistent with the data we must take $c \approx 0.25$. The nuclear saturation scale given by eq. (B.8) is too small to be consistent with measurements by other groups.

In fig. 5, we show the NMC data on the ratio of structure functions as a function of A now using the MV initial condition with anomalous dimension $\gamma = 1.13$. We find that for $c = 0.5$ this fits the data rather well. Based on the above results, for nuclei we will use the MV model and take $\gamma = 1.13$ and $Q_{s0}^2 = 0.5 A^{1/3} Q_{s0,p}^2$. Therefore we have $Q_{s0}^2 = 0.17, 0.26, 0.37$ and 0.44 (GeV)² for C, Ca, Sn and Au respectively. Note that these values of the saturation scale are for quarks in the fundamental representation. For gluons

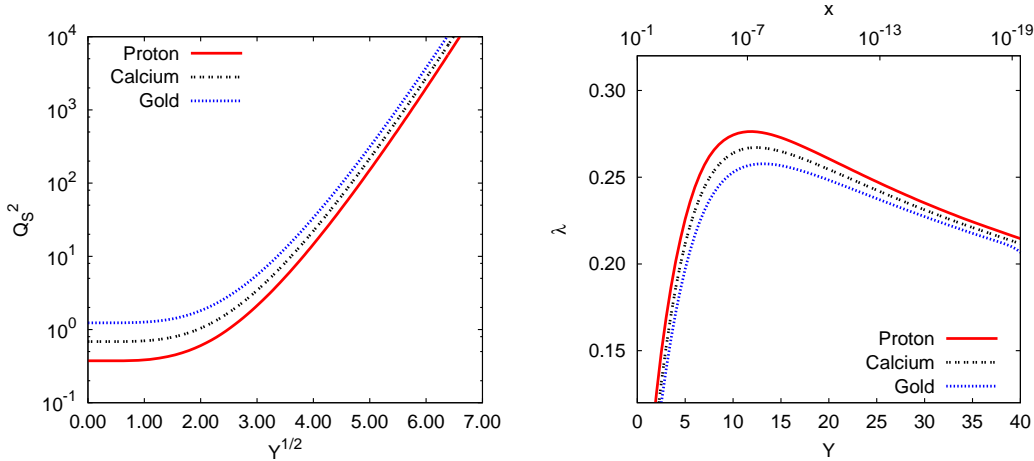


Figure 9: Left: The saturation scale Q_s as a function of the square root of the rapidity $Y^{1/2}$ for protons, calcium and gold nuclei. Note that the slopes of the three curves approach the same value at large Y . Right: $\lambda = d \ln Q_s^2 / dY$ as a function of Y approaches a universal value at large Y .

in the adjoint representation, the corresponding saturation scale is

$$(Q_s^2)_g = \frac{N_c}{C_F} (Q_s^2)_q = 2.25 (Q_s^2)_q \quad (\text{B.9})$$

For gold nuclei this yields $(Q_s^2)_g \approx 1 \text{ GeV}^2$ at $x = 0.01$, in fairly close agreement to the value of 1.3 GeV^2 obtained in [18, 70]. Finally, we plot in fig. 9 (left) the saturation scale in the running coupling case as a function of $Y^{1/2}$ for the proton, calcium and gold nuclei. The behavior at small $Y^{1/2}$ is sensitive to the initial conditions of each of these nuclei; however, at large $Y^{1/2}$ (small x) the curves of the three nuclear approach the same slope, as one expects asymptotically for the behavior of Q_s when running coupling effects are accounted for (see also [71]). The same trend can be observed by plotting (see fig. 9 right) $\lambda = d \ln Q_s^2 / dY$, the parameter that sets the rate at which the dipole amplitudes evolve with rapidity. These results confirm the universal behavior at large Y predicted in Ref. [72].

References

- [1] F. Gelis, T. Lappi, R. Venugopalan, Phys. Rev. **D 79**, 094017 (2009).
- [2] L.D. McLerran, R. Venugopalan, Phys. Rev. **D 49**, 2233 (1994).
- [3] L.D. McLerran, R. Venugopalan, Phys. Rev. **D 49**, 3352 (1994).
- [4] L.D. McLerran, R. Venugopalan, Phys. Rev. **D 50**, 2225 (1994).
- [5] J. Jalilian-Marian, A. Kovner, L.D. McLerran, H. Weigert, Phys. Rev. **D 55**, 5414 (1997).
- [6] J. Jalilian-Marian, A. Kovner, A. Leonidov, H. Weigert, Nucl. Phys. **B 504**, 415 (1997).
- [7] J. Jalilian-Marian, A. Kovner, A. Leonidov, H. Weigert, Phys. Rev. **D 59**, 014014 (1999).
- [8] J. Jalilian-Marian, A. Kovner, A. Leonidov, H. Weigert, Phys. Rev. **D 59**, 034007 (1999).

- [9] J. Jalilian-Marian, A. Kovner, A. Leonidov, H. Weigert, Erratum. Phys. Rev. **D 59**, 099903 (1999).
- [10] E. Iancu, A. Leonidov, L.D. McLerran, Nucl. Phys. **A 692**, 583 (2001).
- [11] E. Iancu, A. Leonidov, L.D. McLerran, Phys. Lett. **B 510**, 133 (2001).
- [12] E. Ferreira, E. Iancu, A. Leonidov, L.D. McLerran, Nucl. Phys. **A 703**, 489 (2002).
- [13] T. Lappi, L.D. McLerran, Nucl. Phys. **A 772**, 200 (2006).
- [14] F. Gelis, R. Venugopalan, Acta Phys. Polon. **B 37**, 3253 (2006).
- [15] F. Gelis, T. Lappi, R. Venugopalan, Int. J. Mod. Phys. E **16**, 2595 (2007).
- [16] L.V. Gribov, E.M. Levin, M.G. Ryskin, Phys. Rept. **100**, 1 (1983).
- [17] A.H. Mueller, J-W. Qiu, Nucl. Phys. **B 268**, 427 (1986).
- [18] H. Kowalski, T. Lappi, R. Venugopalan, Phys. Rev. Lett. **100**, 022303 (2008).
- [19] B. Alver, et al., [PHOBOS Collaboration] arXiv:0903.2811.
- [20] B.I. Abelev, et al., [STAR Collaboration] arXiv:0909.0191.
- [21] F. Gelis, R. Venugopalan, Nucl. Phys. **A 776**, 135 (2006).
- [22] F. Gelis, R. Venugopalan, Nucl. Phys. **A 779**, 177 (2006).
- [23] F. Gelis, T. Lappi, R. Venugopalan, Phys. Rev. **D 78**, 054019 (2008).
- [24] F. Gelis, T. Lappi, R. Venugopalan, Phys. Rev. **D 78**, 054020 (2008).
- [25] A. Krasnitz, R. Venugopalan, Phys. Rev. Lett. **84**, 4309 (2000).
- [26] A. Krasnitz, R. Venugopalan, Phys. Rev. Lett. **86**, 1717 (2001).
- [27] A. Krasnitz, R. Venugopalan, Nucl. Phys. **B 557**, 237 (1999).
- [28] A. Krasnitz, Y. Nara, R. Venugopalan, Nucl. Phys. **A 727**, 427 (2003).
- [29] A. Krasnitz, Y. Nara, R. Venugopalan, Phys. Rev. Lett. **87**, 192302 (2001).
- [30] A. Krasnitz, Y. Nara, R. Venugopalan, Phys. Lett. **B 554**, 21 (2003).
- [31] T. Lappi, Phys. Rev. **C 67**, 054903 (2003).
- [32] T. Lappi, Phys. Rev. **C 70**, 054905 (2004).
- [33] T. Lappi, Phys. Lett. **B 643**, 11 (2006).
- [34] A. Dumitru, F. Gelis, L. McLerran, R. Venugopalan, Nucl. Phys. **A 810**, 91 (2008).
- [35] S. Gavin, L. McLerran, G. Moschelli, Phys. Rev. **C 79**, 051902 (2009).
- [36] G. Moschelli, S. Gavin, L.D. McLerran, Eur. Phys. J. **C 62**, 277 (2009).
- [37] K. Rummukainen, H. Weigert, Nucl. Phys. **A 739**, 183 (2004).
- [38] I. Balitsky, Phys. Rev. **D 70**, 114030 (2004).
- [39] Yu.V. Kovchegov, Phys. Rev. **D 55**, 5445 (1997).
- [40] Yu.V. Kovchegov, J. Kuokkanen, K. Rummukainen, H. Weigert, Nucl. Phys. **A 823**, 47 (2009).

- [41] I. Balitsky, G.A. Chirilli, Phys. Rev. **D 77**, 014019 (2008).
- [42] Yu.V. Kovchegov, H. Weigert, Nucl. Phys. **A 784**, 188 (2007).
- [43] J.L. Albacete, N. Armesto, J.G. Milhano, C.A. Salgado, Phys. Rev. **D 80**, 034031 (2009).
- [44] J.L. Albacete, N. Armesto, J.G. Milhano, C.A. Salgado, arXiv:0906.2721.
- [45] T. Lappi, Acta Phys. Polon. **B 40**, 1997 (2009).
- [46] F. Gelis, T. Lappi, R. Venugopalan, arXiv:0907.4381 [hep-ph].
- [47] H. Fujii, F. Gelis, R. Venugopalan, Nucl. Phys. **A 780**, 146 (2006).
- [48] A. Kovner, L.D. McLerran, H. Weigert, Phys. Rev. **D 52**, 3809 (1995).
- [49] Yu.V. Kovchegov, D.H. Rischke, Phys. Rev. **C 56**, 1084 (1997).
- [50] E.A. Kuraev, L.N. Lipatov, V.S. Fadin, Sov. Phys. JETP **45**, 199 (1977).
- [51] I. Balitsky, L.N. Lipatov, Sov. J. Nucl. Phys. **28**, 822 (1978).
- [52] J.P. Blaizot, F. Gelis, R. Venugopalan, Nucl. Phys. **A 743**, 13 (2004).
- [53] H. Fujii, F. Gelis, R. Venugopalan, Phys. Rev. Lett. **95**, 162002 (2005).
- [54] Yu.V. Kovchegov, A.H. Mueller, Nucl. Phys. **B 529**, 451 (1998).
- [55] M.A. Braun, Phys. Lett. **B 483**, 105 (2000).
- [56] T. Lappi, S. Srednyak, R. Venugopalan, arXiv:0911.2068 [hep-ph].
- [57] K. Dusling, D. Fernandez-Fraile, R. Venugopalan, Nucl. Phys. **A 828**, 161 (2009).
- [58] M. A. Braun, Eur. Phys. J. C **55**, 377 (2008) [arXiv:0801.0493 [hep-ph]].
- [59] M. Ciafaloni, G. Marchesini, Nucl. Phys. **B 109**, 261 (1976).
- [60] J.P. Blaizot, F. Gelis, R. Venugopalan, Nucl. Phys. **A 743**, 57 (2004).
- [61] L.N. Lipatov, Phys. Rept. **286**, 131 (1997).
- [62] J.L. Albacete, Y. Kovchegov, Phys. Rev. **D 75**, 125021 (2007).
- [63] P. Amaudruz, et al., [New Muon Collaboration] Nucl. Phys. **B 441**, 3 (1995).
- [64] M. Arneodo, et al., [NMC Collaboration] Nucl. Phys. **B 481**, 3 (1996).
- [65] K. Golec-Biernat, M. Wüsthoff, Phys. Rev. **D 59**, 014017 (1999).
- [66] F. Gelis, A. Stasto, R. Venugopalan, Eur. Phys. J. **C 48**, 489 (2006).
- [67] J.H. Lee, [for the BRAHMS Collaboration] Mini-Symposium on Collective Flow in Relativistic Heavy Ion Collisions, APS/DNP 2003, Tucson, Arizona.
- [68] M. Murray, [for the BRAHMS collaboration] PoS, **HEP2005**, 127 (2006).
- [69] R. Debbe, [for the BRAHMS Collaboration] AIP Conf. Proc. **698**, 690 (2004).
- [70] H. Kowalski, D. Teaney, Phys. Rev. **D 68**, 114005 (2003).
- [71] J.L. Albacete, N. Armesto, J.G. Milhano, C.A. Salgado, U.A. Wiedemann, Phys. Rev. **D 71**, 014003 (2005).
- [72] A.H. Mueller, Nucl. Phys. **A 724**, 223 (2003).